

JUST SAY THE NAME: ONLINE CONTINUAL LEARNING WITH CATEGORY NAMES ONLY VIA DATA GENERATION

Minhyuk Seo^{1,2}
Hyeonbeom Choi²

Seongwon Cho²
Seon Joo Kim¹

Minjae Lee²
Jonghyun Choi²

Diganta Misra^{3,4}

¹Yonsei University ²Seoul National University ³MPI-IS Tübingen ⁴ELLIS Tübingen
{minhyukseo, seonjookim}@yonsei.ac.kr, diganta.misra@mila.quebec,
{seongwoncho, mj1020, gusqja1228, jonghyunchoi}@snu.ac.kr

ABSTRACT

Requiring extensive human supervision is often impractical for continual learning due to its cost, leading to the emergence of ‘name-only continual learning’ that only provides the name of new concepts (*e.g.*, classes) without providing supervised samples. To address the task, recent approach uses web-scraped data but results in issues such as data imbalance, copyright, and privacy concerns. To overcome the limitations of both human supervision and webly supervision, we propose *Generative name only Continual Learning (GenCL)* using generative models for the name only continual learning. But naïve application of generative models results in limited diversity of generated data. So, we specifically propose a diverse prompt generation method, Hierarchical Recurrent Prompt Generation (**HIRPG**) as well as COMplexity-NAvigating eNsembler (**CONAN**) that selects samples with minimal overlap from multiple generative models. We empirically validate that the proposed GenCL outperforms prior arts, even a model trained with fully supervised data, in various tasks including image recognition and multi-modal visual reasoning. Data generated by GenCL is available at <https://anonymous.4open.science/r/name-only-continual-E079>

1 INTRODUCTION

Continual learning (CL) has been addressing various domains across different modalities including computer vision (Seo et al., 2024b), natural language processing (Wu et al., 2024b), and multimodal learning (He et al., 2023a). But even the most existing methods (Wang et al., 2022; Kim et al., 2024a) often rely on abundant well-curated human supervision. For example, obtaining 423.5k clean images in DomainNet (Neyshabur et al., 2020) required 50,000 working hours to manually filter out outliers.

In standard learning, where all training data are provided at once, the time allocated for data collection and preprocessing does not affect performance, since these steps are completed before model training begins. In contrast, continual learning involves the continuous encounter of new ‘concepts’, which can refer to classes, adjectives, and verbs in multi-modal tasks, necessitating ongoing data preparation throughout training. Therefore, delays in preparing data for encountered concepts hinder the model’s ability to quickly adapt to new concepts (Koh et al., 2021; Caccia et al., 2022). Consequently, delays in data preparation, such as human annotation, could limit the applicability of CL method in deployment, such as e-commerce recommendation systems and autonomous driving.

In recent literature, several alternatives to human annotation have been proposed. Madaan et al. (2021) propose an unsupervised CL setup that eliminates the need for annotation. However, they assume that the unlabeled data stream contains only data related to the target concepts, while in real-world scenarios, unlabeled data often include irrelevant data, which can potentially hinder the performance of the target concept (Halevy et al., 2016; Yang et al., 2023). As another alternative to human-annotated data, Sato (2023); Prabhu et al. (2024) proposes the use of web-scraped data for online learning. Although web-scraped data presents advantages such as abundance (Xu et al., 2024), diversity (Agun, 2023), and easy accessibility (Sun et al., 2018), challenges arise from privacy and copyright concerns (Zhang et al., 2023a), as well as inherent noise (Neyshabur et al., 2020), which significantly hinders the performance of continual learner (Kim et al., 2021; Bang et al., 2022).

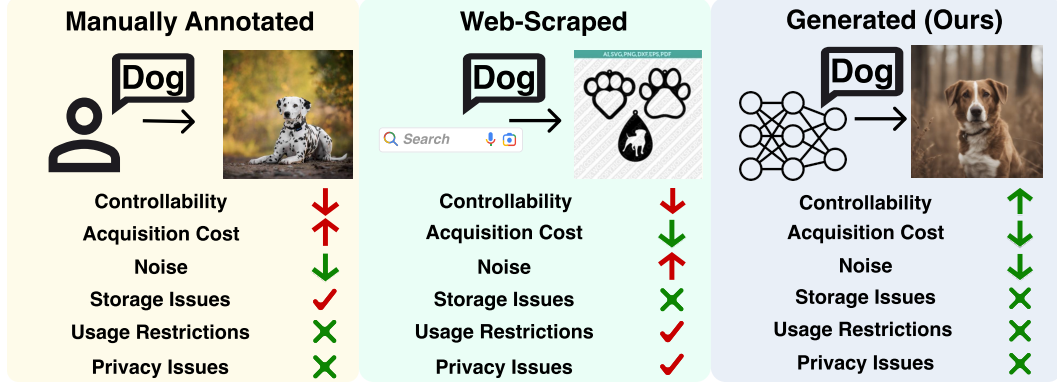


Figure 1: **Comparison of Manually Annotated (MA) data, Web-Scraped Data, and Generated data.** Generated data addresses constraints associated with Web-scraped or MA data, mitigating privacy concerns and usage restrictions (*i.e.*, whether images can be used for learning). Also, it maintains controllability (the ability to generate images with various contexts, *e.g.*, background, color) as desired. Generated data are less noisy (*i.e.*, containing fewer undesired images) than web-scraped data and proves to be a more cost-effective than MA data which requires human annotation. For more details on the terminology employed in this figure, see Sec. A.19

To address those issues, we propose to leverage text-to-image (T2I) generative models for CL. Specifically, we propose *Generative name only Continual Learning (GenCL)*, which takes only *concepts* as input and trains on images generated by text-to-image (T2I) generative models based on the given *concepts*. It takes advantage of generative models, such as controllability (Nie et al., 2021) (*i.e.*, generating desired data), unlimited image generation (Liang et al., 2022), and addressing privacy concerns (Shin et al., 2017), as illustrated in Fig. 1. Additionally, it significantly accelerates the data collection process; for example, generating DomainNet using SDXL (Podell et al., 2023) with 8 NVIDIA RTX 4090 GPUs take only 80 hours, compared to the 50,000 hours required for manual annotation.

However, generated images often suffer from limited diversity (Tian et al., 2024a; Bianchi et al., 2023; Fraser et al., 2023). To address this issue, we define *intra-diversity* and *inter-diversity*, which refers to the diversity of data generated by a single T2I model and the diversity of data generated by multiple T2I models, respectively. Specifically, to improve intra-diversity, we propose Hierarchical Recurrent Prompt Generation (**HIRPG**), a diverse prompt generation method that utilizes the in-context learning capabilities of Large Language Models (LLMs) to generate a diverse set of text prompts. To improve the inter-diversity, we propose a complexity-guided data ensemble method, named Complexity-NAvigating eNsembler (**CONAN**). CONAN not only ensembles data from multiple generative models, but also selects a coreset, and trains a model exclusively on this coreset to improve training efficiency for real-time adaptation to new concepts. We empirically demonstrate that our framework significantly outperforms baselines in both class-incremental and multi-modal visual concept-incremental setups.

In sum, we aim to address the following research questions, thus summarizing our core contributions as follows:

- RQ1. *Can generated data substitute manually annotated (MA) in CL setups?* **GenCL** improves A_{AUC} on the PACS (Zhou et al., 2020) OOD domain by 9% and 13% over the model trained with web-scraped and MA data, respectively.
- RQ2. *How to ensure diversity of images generated from generative models?* We propose **HIRPG**, a prompt generation method that takes advantage of LLM to create diverse text prompts for a given concept, which are subsequently used by T2I models to generate images.
- RQ3. *How to ensemble generated data from a set of generators?* We propose **CONAN**, a data selection method that accounts for the complexity of generated samples.

2 RELATED WORK

2.1 CONTINUAL LEARNING

Setups for Continual Learning. Many recent works propose realistic CL scenarios, such as blurry (Prabhu et al., 2020; Bang et al., 2021), i-blurry (Koh et al., 2021), continuous (Shanahan

et al., 2021; Koh et al., 2023), and noisy (Bang et al., 2022) setups. However, they only focus on the realistic data distribution of the stream data, rather than the acquisition of data for a new category, for which the model needs to be learned. Recently, C2C (Prabhu et al., 2024) used web-scraped data for continual learning, to address the high cost of manual data annotation and the difficulty in acquiring real-time data for the target concepts the model needs to learn. However, web-scraped data present several limitations, including privacy concerns, usage restrictions, and inherent noise, as highlighted in Fig. 1. Please refer to Sec. A.19 for more comparison between web data and generated data.

2.2 DATA SELECTION

For ensembling generated images from multiple T2I generative models, we consider data selection methods that extract most essential samples to build a coreset from a larger candidate set. Formally, from the candidate set T , these methods select a coreset V ($|V| \ll |T|$), aiming to preserve as much task-relevant information from T as possible (Shin et al., 2023). To estimate the informativeness of the candidates, several metrics have been proposed, such as gradient (Paul et al., 2021; Pooladzandi et al., 2022; Shin et al., 2023), uncertainty (Coleman et al., 2020), influential score (Yang et al., 2022a; Pooladzandi et al., 2022), and distance (Xia et al., 2023).

Although these methods are effective at selecting coresets, many come with substantial computational costs. Gradient-based methods (Paul et al., 2021; Pooladzandi et al., 2022; Shin et al., 2023), which aim to minimize the difference between the gradients of the training dataset T and the selected set V , require a well-trained model on T , which significantly increases computational overhead. Similarly, the influence score-based method (Yang et al., 2022a) also requires significant computation due to the necessity of calculating the Hessian in the influence function, along with its iterative data selection process (Xia et al., 2023). In contrast, distance-based methods, such as Xia et al. (2023) and our proposed CONAN, can directly leverage a well-trained feature extractor, *i.e.*, requiring only model forward passes for feature extraction, leading to faster data preparation time.

2.3 TRAINING WITH TEXT-TO-IMAGE (T2I) GENERATIVE MODELS

With the availability of robust generative models (Gu et al., 2023; Tang et al., 2023; Podell et al., 2023), several recent studies have utilized synthetic data for training (Azizi et al., 2023; Tian et al., 2024a; Zhang et al., 2024c; Tian et al., 2024b). Notably, (Tian et al., 2024a) demonstrate the positive impact of using diffusion model-generated datasets at ImageNet (Deng et al., 2009) scale for training.

To train a model with data generated by T2I generative models for a given concept c , concept-specific prompts p_c are needed. Ramesh et al. (2022); Jones et al. (2024) use the template "A photo of a c ", as proposed in CLIP (Radford et al., 2021), to construct prompt for concept c . However, Saryıldız et al. (2023) claim that using only the class name as a prompt ($p_c = "c"$) yields better image generation than $p_c = "A photo of a c"$. To add more concept-specific context to p_c , Saryıldız et al. (2023) combine the concept name c with its definition d_c from WordNet (Miller, 1995), resulting in $p_c = "c, d_c"$. Nonetheless, all these approaches rely on a single type of p_c per concept, limiting the diversity of generated images despite the ability of T2I models to generate an unlimited number of images (Vardanyan et al., 2024; Tian et al., 2024a).

To address the limited diversity in generated images, several prompt diversification methods have been proposed. LE (He et al., 2023b) leverages a pre-trained word-to-sentence T5 model (Raffel et al., 2020) to generate diverse sentences that incorporate class names. Furthermore, Saryıldız et al. (2023) integrates the concept's hypernym h_c from WordNet, along with a background scene b from the 365 scenes in Places365 (López-Cifuentes et al., 2020), resulting in $p_c = "c, h_c \text{ inside } b"$. In contrast to random background selection, Tian et al. (2024a) utilize LLM to generate a list of contextually appropriate backgrounds for the given concept c to create more plausible prompts. Similarly, Hammoud et al. (2024) and our proposed diverse prompt generation method, HIRPG, also employ an LLM-based prompt generator. However, while previous LLM-based prompt generation methods do not account for the relationship between generated prompts, HIRPG minimizes overlap between them by providing previously generated prompts as negative examples to the LLM.

We review more relevant literature and provide extended related work in Sec. A.18 for space's sake.

3 PROBLEM STATEMENT OF NAME ONLY CONTINUAL LEARNING

In the name-only CL setup (Prabhu et al., 2024), only new concepts to be learned, denoted $\mathcal{Y} = \{y_1, y_2, \dots\}$, are provided in a streaming manner, while the prevalent online continual learning setups assume well-curated annotated data $(\mathcal{X}, \mathcal{Y})$ are given. The objective of this setup is to train a model f_θ , parameterized by θ , to classify the data into the concepts seen up to the given time step t , *i.e.*, $\{y_i\}_{i=1}^t$. To train f_θ for the given concepts, the learner can access either public data, such as data scraped on the Web (Prabhu et al., 2024), or generated data. To evaluate whether the model f_θ learns concepts $\{y_i\}_{i=1}^t$ at the time step t , curated data $\{\mathcal{X}_i, y_i\}_{i=1}^k$ are used, where \mathcal{X}_i refers to the set of data that corresponds to the category y_i .

4 APPROACH

We propose a Generative name only Continual Learning (**GenCL**) framework to address the absence of data in the name-only CL setup. The GenCL framework is composed of four integral components: (i) a Prompt Generation Module ψ (Sec. 4.1), (ii) a set of Generators \mathcal{G} (Sec. 4.2), (iii) an Ensembler Δ (Sec. 4.3), and (iv) a learner f_θ . We illustrate an overview of GenCL in Fig. 2.

When a new concept is introduced, for which f_θ needs to be learned, a generator $g \in \mathcal{G}$ generates images related to the concept. However, despite generative models being capable of producing an unlimited number of images, output diversity is often limited (Liu et al., 2023a; Sadat et al., 2023). To address this, we employ a prompt generation module ψ , which generates diverse text prompts and forwards them to the T2I generative models. Additionally, we further enhance the diversity of the generated images by utilizing a proposed ensemble approach that combines the outputs of a set of generators \mathcal{G} through ensembler Δ . Generated images are streamed to the learner f_θ in real-time, while a finite episodic memory is maintained to replay previously encountered data. Note that unlike real data (*e.g.*, web-scraped data), storing samples in episodic memory is free from data privacy issues. While it is possible to generate data for past concepts in real-time without using episodic memory, we use it for efficiency, as it allows for reducing computational costs without privacy concerns.

4.1 PROMPT GENERATION MODULE (ψ)

Our pipeline ψ begins with the new concept as input and constructs a base prompt P_B using the template: ‘A photo of [concept]’ following (Shtedritski et al., 2023; Shi et al., 2023). While this base prompt can be used directly with the T2I generators \mathcal{G} , generating images using a single prompt may lead to limited diversity in style, texture, and backgrounds across the generated images (Fan et al., 2024). To enhance diversity, we generate additional diverse prompts using LLMs.

A straightforward approach for diverse prompt generation using LLMs is to generate N different prompts at once or to generate a single prompt N times, as in previous work (He et al., 2023b; Hammoud et al., 2024). However, multiple inferences to LLM with the same input can produce similar outputs (Zhang et al., 2024a; Skapars et al., 2024), despite the non-deterministic nature of LLM (Song et al., 2024). Empirically, as shown in Sec. A.25, our observations indicate that using these approaches often leads to many generated prompts with similar meanings, which may reduce the diversity of the generated images from T2I generative models.

To reduce overlap between generated prompts, we iteratively create new prompts that are distinct from those produced in previous steps. Inspired by previous work that has shown improved performance in solving complex problems by providing negative examples with positive examples in in-context learning (Zhang et al., 2024b) and contrastive Chain-of-Thought (Chia et al., 2023), we incorporate previously generated prompts into the LLM input to serve as negative examples. By presenting these previously generated prompts and requesting a new prompt that is distinct from them, we impose a hard constraint that effectively prevents overlap between the newly generated prompts and the previous ones. Formally, this process can be described as follows:

$$P_i = \begin{cases} \text{LLM}(P_S, P_B) & i = 1 \\ \text{LLM}(P_S, \{P_B\} \cup \{P_m\}_{m=1}^{i-1}) & i \geq 2, \end{cases} \quad (1)$$

which takes the system prompt P_S and all previously generated prompts $\{P_m\}_{m=1}^{i-1}$ as input. Since there are no negative examples in the initial step (*i.e.*, $i = 1$), we use the base prompt P_B as the initial

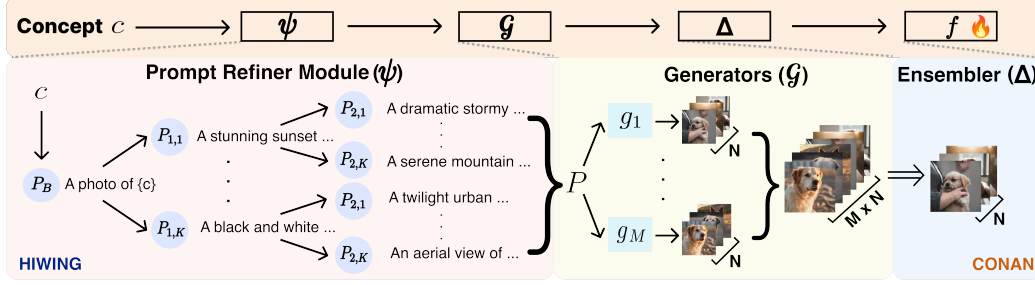


Figure 2: **Illustration of the proposed GenCL framework.** When a new concept that needs to be learned is encountered, it is passed through a prompt generation module, ψ , to produce diverse prompts. These prompts are then used to generate data from a set of generators, \mathcal{G} . The data generated by each generator are combined through the ensembler, Δ , and subsequently used to train the model, f_θ .

negative example, where $P_B = \text{'A photo of [concept]'}$. To generate N different prompts, we repeat the process N times. As previously generated prompts are iteratively used as negative examples, we name this process as Recurrent Prompt Generation (RPG). The system prompt P_S we use is as follows:

To generate images using a text-to-image generative model, I need to create a prompt ~~~
Here is a list of prompts that I have previously generated. Please create a new prompt that does not overlap with {base prompt & previously generated prompts} ~~~.

However, generating a large number of prompts using RPG poses a challenge. As the iterative steps are repeated, the length of the LLM input for in-context learning (ICL) increases, which can lead to difficulties in fully utilizing information within the long context, a problem known as *lost-in-the-middle challenge* (An et al., 2024; Liu et al., 2024), as well as substantial computational overhead in long-context ICL (Li et al., 2024).

To address this challenge, we divide the RPG into multiple subtasks using a hierarchical tree structure. Specifically, we construct a complete K -ary tree (Gross et al., 2018), where every internal node has exactly K child nodes. Each node represents a prompt, with the root node (*i.e.*, the node at depth 0) defined as $P_B = \text{'A photo of [concept]'}$. To generate the K child nodes at depth 1, we first perform RPG. To generate more diverse prompts, we extend the tree to depth 2, again using RPG, with each parent node at depth 1 serving as the base prompt P_B in Eq. 1, and this process continues for subsequent depths. Formally, focusing on the k^{th} child node at depth d , denoted as $P_{d,k}$ ($d \geq 0, 1 \leq k \leq K$), its child nodes $P_{d+1,k'}$ ($1 \leq k' \leq K$) are generated through the RPG as follows:

$$P_{d+1,k'} = \begin{cases} \text{LLM}(P_S, P_{d,k}) & k' = 1 \\ \text{LLM}(P_S, \{P_{d,k}\} \cup \{P_{d+1,m}\}_{m=1}^{k'-1}) & 2 \leq k' \leq K, \end{cases} \quad (2)$$

where $\{P_{d+1,m}\}_{m=1}^{k'-1}$ refers to the previously generated nodes that share the same parent node $P_{d,k}$. By constructing complete K -ary Tree with a depth of D , we can generate $\frac{K^{D+1}-1}{K-1}$ nodes (*i.e.*, prompts), which includes all internal and leaf nodes. This hierarchical generation enables us to generate diverse prompts while bounding the number of negative examples by K ($\ll N$), thereby addressing both the *lost-in-the-middle challenge* and the computational overhead. We name this proposed diverse prompt generation process as Hierarchical Recurrent Prompt Generation (**HIRPG**).

Since we divide RPG into subtasks using a hierarchical tree structure, we cannot consider nodes generated from different branches as negative examples during the RPG in each node. Nonetheless, overlap between generated prompts from different nodes is rare. This is because RPG in each node begins with a distinct $P_{d,k}$ in Eq. 2, serving as a negative example in the first step ($k' = 1$), and different examples in in-context learning lead to varied outputs (Su et al., 2022; Agarwal et al., 2024). We empirically demonstrate the effectiveness of HIRPG by comparing it quantitatively and qualitatively with existing prompt generation methods in Sec.5.2 and Sec.A.25, respectively. We provide a pseudocode for the prompt diversification module ψ in Algorithm 3 in the appendix.

4.2 GENERATORS (\mathcal{G})

In addition to enhancing intra-diversity, we amplify the inter-diversity, the diversity between images generated by multiple T2I generative models, by ensembling the images generated by these models. Specifically, using a T2I generator $g_i(\cdot) \in \mathcal{G}$ and a prompt set \mathbf{P} generated by ψ , we generate a set of images $U_i = g_i(\mathbf{P})$. At the end of generation, we have $\mathbf{U} = \bigcup_{i=1}^{|\mathcal{G}|} U_i$, the union of images generated by $|\mathcal{G}|$ generative models, with the same number of images generated for each model, *i.e.*, $|U_1| = |U_2| = \dots = |U_{|\mathcal{G}|}|$. We provide detailed information about the generators we employ, including examples of generated images from each generator in Sec. A.17.

4.3 ENSEMBLER (Δ)

When ensembling images generated by different T2I models, a key question arises: *Do we need to use all of them?* While large-scale training datasets have become standard for achieving state-of-the-art deep learning models (Zhao et al., 2021; Yang et al., 2022b), training with massive data imposes not only computational burden and time complexity (Sharir et al., 2020; Kim et al., 2022), but also significant energy and carbon footprint (Schwartz et al., 2020; Patterson et al., 2021). In addition, in CL setups, prolonged training periods can hinder fast adaptation to new concepts (Seo et al., 2024a).

Therefore, we aim to select a coreset \mathbf{V} from the entire generated data \mathbf{U} , and train a learner only using \mathbf{V} . Specifically, we select $|U_i|$ ($U_i \in \mathbf{U}$) samples from \mathbf{U} for \mathbf{V} to maintain the same training cost as using data generated by a single generative model while increasing the diversity of the ensemble set. A straightforward selection method for constructing \mathbf{V} is to sample images from each generator with equal weights. However, surprisingly, this method degrades the performance of models trained with ensembled images, even compared to those trained on images from a single generative model (*i.e.*, no ensembling), as shown in Tab. 3. This degradation occurs because the equal-weight selection method does not account for the overlap between images, *i.e.*, diversity.

To enhance diversity in the ensembled set, we select samples positioned far from the class prototype in the feature space, *i.e.*, *difficult samples*, since these images are less likely to overlap with common images compared to those that are closer to the prototype. To achieve this, we consider the class-wise Mahalanobis distance (Mahalanobis, 2018), where a higher distance indicates that a sample is farther from the class prototype. However, it only accounts for the class-specific difficulty, while the distance from other classes can also affect the difficulty of samples. For example, consider two samples, x_1 and x_2 , both belonging to class c and having the same class-wise Mahalanobis distance. If x_1 is closer to the global prototype (*i.e.*, the class-agnostic prototype) than x_2 , then x_1 may be more challenging to classify as class c , since x_1 is more likely to be confused with other classes. Therefore, to select difficult samples in the ensemble set while considering for both class-wise difficulty and their relationship to other classes, we employ the relative Mahalanobis distance (RMD) score (Ren et al., 2021). It measures the *difficulty* in classifying a sample into its corresponding class by comparing the distance from the class prototype with the distance from the global prototype (Cui et al., 2023). The RMD score for a sample $(x_i, y_i) \in \mathbf{U}$ is given by the following:

$$\begin{aligned} \mathcal{RMD}(x_i, y_i) &= \mathcal{M}(x_i, y_i) - \mathcal{M}_{\text{agn}}(x_i), \\ \mathcal{M}(x, y) &= D_M \left(g(x), \frac{1}{|\mathbf{U}_y|} \sum_{j \in \mathbf{U}_y} f(x_j) \right), \quad \mathcal{M}_{\text{agn}}(x) = D_M \left(g(x), \frac{1}{|\mathbf{U}|} \sum_{j \in \mathbf{U}} f(x_j) \right), \end{aligned} \quad (3)$$

where $g(x)$ refers to the penultimate feature of the feature extractor g , D_M refers to the Mahalanobis distance (MD), \mathbf{U}_y denotes the set of samples belonging to class y , $\mathcal{M}(x_i, y_i)$ and $\mathcal{M}_{\text{agn}}(x_i)$ represents class-wise MD and class-agnostic MD (*i.e.*, global MD), respectively. If a sample is close to the class prototype but far from the global prototype (*i.e.*, low RMD score), it is easy to classify correctly. Conversely, if it is far from the class prototype but close to the global prototype (*i.e.*, high RMD score), the sample is hard to classify correctly and may belong to other near-classes. We show samples with low RMD scores and samples with high RMD scores in Fig. 3.

Measuring the difficulty using the RMD score, we select images with high RMD scores, which are expected to exhibit a widespread dispersion from the class prototype. However, in the coreset, which is a representative subset of an entire dataset (Anonymous, 2023), it is necessary to include not only samples near the decision boundary, but also class-representative samples (Bang et al., 2021; Harun et al., 2023). Therefore, we adopt a probabilistic approach to ensemble selection, rather than simply

choosing images with the k -highest RMD scores, to incorporate class-representative samples into the ensemble set. Specifically, we calculate $p_{u|c}$, the selection probability for sample u to be included in the coreset of class c , with details provided below.

First, we truncate the samples with RMD scores in the upper and lower $L\%$ to minimize the impact of outliers on the probability distribution. Next, we normalize the scores using Z-score normalization and apply a softmax function to obtain the selection probability as:

$$p_{u|c} = \frac{e^{\bar{RMD}_{u|c}/\tau}}{\sum_{u' \in \mathbf{U}_c} e^{\bar{RMD}_{u'|c}/\tau}}, \quad (4)$$

where \mathbf{U}_c refers to the set of samples for class c , $\bar{RMD}_{u|c}$ represents the normalized RMD score for sample $u \in \mathbf{U}_c$, and τ denotes the temperature parameter. Using the selection probability, we not only sample complex samples, but also incorporate a small portion of class-representative samples into the ensemble set. We name our proposed RMD-based probabilistic ensemble method as CComplexity-NAVigating eNsembler (**CONAN**).

We compare CONAN with various RMD-based ensemble methods and existing coreset selection methods in Sec.A.14 and Sec.5.2, respectively. Furthermore, we provide additional justification for using the RMD score in Sec. A.13.

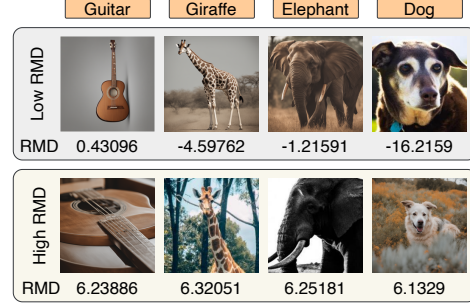


Figure 3: Samples with high RMD scores and low RMD scores

5 EXPERIMENTS

5.1 EXPERIMENTAL SETUP

Continual Learning Setups. We first empirically validate the efficacy of our GenCL by comparing it with state-of-the-art methods in class-incremental learning (CIL) task setups. Beyond CIL setups, we also assess GenCL in multi-modal visual-concept incremental learning (MVCIL). In MVCIL, concepts to be learned (e.g., ‘ride a bike’, ‘kick a ball’) are encountered incrementally. To learn a concept, both positive and negative support sets are required, where the positive set contains images representing the concept, while the negative set contains images that do not. We consider two types of tasks that address the following queries: (1) *What is the concept exclusively depicted by the positive support set?* and (2) *Give a query image, does the query image belong to the positive or negative support set?* We refer to these tasks as CA (Concept Answering) and P/N, respectively. We provide a detailed explanation of the MVCIL setup in Sec. A.1.

Models. We use ResNet-18 and ImageNet-1K pretrained ViT-base as the network architecture for the CIL setup. For the MVCIL setup, we fine-tune the LLaVA-1.5-7B model (Liu et al., 2023b). Specifically, following Ye et al. (2023); Dong et al. (2024), we fine-tune only the pretrained projection MLP layers and LoRA adapters (Hu et al., 2021), keeping the LLM frozen for training efficiency. In all experiments, we train a model with ER (Rolnick et al., 2019), which is a simple but strong CL method (Prabhu et al., 2023; Seo et al., 2024a).

Datasets. We evaluate the domain generalization performance of GenCL in the CIL setup using widely adopted domain generalization (DG) benchmarks: PACS (Zhou et al., 2020), NICO (Zhang et al., 2023c) and DomainNet (Neyshabur et al., 2020), dividing them into multiple discrete tasks. Each DG benchmark consists of multiple domain datasets, e.g., PACS includes four domains: Photo, Art, Cartoon, and Sketch. We selected data from one domain (i.e., photo domain) as MA data for each benchmark, to compare GenCL with the oracle scenario, which assumes that manually annotated (MA) data are available for training. During the evaluation, we considered the selected domain as the in-distribution (ID) domain, while the other domains as out-of-distribution (OOD) domains. For details on the task splits for each benchmark, please refer to Sec.A.2 due to space’s sake. For the MVCIL setup, we used Bongard-HOI (Jiang et al., 2022) and Bongard-OpenWorld (Wu et al., 2024a).

Metrics. We report A_{AUC} (Koh et al., 2021; Caccia et al., 2022; Koh et al., 2023) and A_{last} , which measure inference performance at any time and at the end of training, respectively. In MVCIL-CA task setups, to compare model-predicted sentences with ground-truth sentences, we use CiDER (Vedantam et al., 2015), which measures the similarity between generated and ground truth sentences, while also capturing aspects such as grammaticality, saliency, importance, and both precision and recall. Note that for evaluation, we use the test set for seen categories up to that point in time. Please refer to Sec. A.16 for a more detailed explanation of the metrics we used.

Baselines. We compare a model trained using GenCL with models trained using web-scraped data (C2C (Prabhu et al., 2024)), other synthetic data (Glide-Syn(He et al., 2023b), CHB (Sarıyıldız et al., 2023), SC (Tian et al., 2024a), LE (He et al., 2023b), and CCG (Hammoud et al., 2024)), and manually annotated (MA) data. Specifically, CHB, SC, LE, and CCG generate diverse prompts to enhance the variety of generated images. We compare these methods with our proposed diverse prompt generation method, *i.e.*, HIRPG. Furthermore, we integrate prompt generation baselines with our proposed ensemble method (CONAN) to showcase the effectiveness of CONAN, as well as to provide a fair comparison with GenCL, which leverages multiple generators for ensembling.

Next, we extend GenCL to a standard learning setup (*i.e.*, joint training), where all concepts to be learned are provided at once. In this setup, we compare a model trained with data generated by GenCL to models trained with web-scraped data, other synthetic data, and manually annotated (MA) data. We also compare with training-free baselines, including CLIP-ZS(Radford et al., 2021), SuS-X-SD(Udandara et al., 2023), CuPL (Pratt et al., 2023), VisDesc (Menon & Vondrick, 2023), and CALIP (Guo et al., 2023), as well as SD-Cif (Li et al., 2023), which utilizes SDXL as a classifier.

Finally, we compare our proposed ensemble selection method, *i.e.*, CONAN, with various baselines for coreset selection, including Uncertainty (Coleman et al., 2020), CRAIG (Mirzasoleiman et al., 2020), Glister (Killamsetty et al., 2021b), GradMatch (Killamsetty et al., 2021a), Ada-core (Pooladzandi et al., 2022), LCMat (Shin et al., 2023), and Moderate (Xia et al., 2023).

For detailed description of training-free name-only classification baselines, prompt generation baselines and data ensemble baselines, see Sec. A.12, Sec. A.10 and Sec. A.11, respectively.

5.2 QUANTITATIVE ANALYSIS

Effectiveness of GenCL in CIL. To assess the effectiveness of our proposed GenCL in a setup, where only concept names are provided without data, we compare its performance against models trained on web-scraped data, other synthetic data, as well as manually annotated data, representing the ideal case. In the CIL setup, we assume that the category names of the PACS and DomainNet datasets are provided incrementally, and we summarize the results not only in the ID domain but also in the OOD domain in Tab. 1. Note that since DomainNet is a web-scraped dataset, sharing the same domain as C2C (Prabhu et al., 2024), which also uses web-scraping for data acquisition, we exclude C2C from the comparison in DomainNet.

In in-distribution (ID) domain, MA outperforms other baselines, as well as GenCL. This is because the ID test set we use is derived from the same test set as the MA data, giving it an advantage in this specific domain. However, in the out-of-distribution (OOD) domains of PACS, CONAN outperforms both MA and other baselines. We believe that we achieve better generalization performance by generating a more diverse set of images through a diversified set of prompts and an ensemble selection of generators. We provide additional comparisons with various combinations of diverse prompt generation baselines and data ensemble methods in Sec. A.26.

Effectiveness of GenCL in MVCIL. We also empirically validate the effectiveness of GenCL in the MVCIL setup, and summarize the result in Tab. 2. Since CHB, SC, and CCG focus solely on image classification tasks, we exclude them from the MVCIL setup. Additionally, Glide-Syn and LE utilize a word-to-sentence model to generate diverse prompts, making them inapplicable to Bongard-OpenWorld, which uses sentences as concepts. Note that while C2C and manually annotated (MA) data utilize human-annotated hard negative concepts alongside the concepts to be learned (*i.e.*, positive concepts), GenCL relies solely on positive concepts. Specifically, to acquire MA data, high-quality annotators from Amazon Mechanical Turk were employed to select hard negative examples and filter out noisy data (Jiang et al., 2022). In contrast, GenCL automatically selects

Method	PACS				DomainNet			
	ID		OOD		ID		OOD	
	$A_{AUC} \uparrow$	$A_{last} \uparrow$	$A_{AUC} \uparrow$	$A_{last} \uparrow$	$A_{AUC} \uparrow$	$A_{last} \uparrow$	$A_{AUC} \uparrow$	$A_{last} \uparrow$
C2C (CoLLAs 2024)	47.29 \pm 2.75	39.23 \pm 3.78	28.33 \pm 1.93	20.77 \pm 1.51	35.06 \pm 0.41	27.81 \pm 0.15	11.89 \pm 0.22	8.82 \pm 0.08
Glide-Syn (ICLR 2023)	34.59 \pm 2.14	32.05 \pm 1.44	31.53 \pm 1.56	26.56 \pm 1.84	15.64 \pm 0.44	10.68 \pm 0.19	4.06 \pm 0.13	2.59 \pm 0.03
LE (ICLR 2023)	46.47 \pm 2.00	45.76 \pm 2.33	32.42 \pm 1.35	27.56 \pm 0.66	20.01 \pm 0.27	15.38 \pm 0.31	6.40 \pm 0.13	4.59 \pm 0.09
(+) CONAN	49.37 \pm 3.77	50.45 \pm 1.56	33.88 \pm 1.79	30.29 \pm 0.81	30.80 \pm 0.63	25.33 \pm 0.20	9.54 \pm 0.25	7.59 \pm 0.17
CHB (CVPR 2023)	47.52 \pm 2.69	46.11 \pm 1.07	31.02 \pm 1.11	22.82 \pm 1.61	16.69 \pm 0.16	13.45 \pm 0.19	5.61 \pm 0.11	4.18 \pm 0.05
(+) CONAN	52.01 \pm 2.72	45.46 \pm 3.27	32.62 \pm 1.72	24.26 \pm 0.89	29.06 \pm 0.37	24.52 \pm 0.17	9.28 \pm 0.14	7.56 \pm 0.14
SC (CVPR 2024)	44.03 \pm 1.95	41.48 \pm 3.05	30.72 \pm 1.19	23.07 \pm 1.04	11.89 \pm 0.17	8.66 \pm 0.20	3.90 \pm 0.07	2.68 \pm 0.04
(+) CONAN	50.45 \pm 2.70	52.35 \pm 0.99	31.04 \pm 1.26	23.90 \pm 1.35	22.36 \pm 0.34	19.13 \pm 0.32	6.71 \pm 0.15	5.48 \pm 0.13
CCG (arXiv 2024)	45.49 \pm 2.81	45.29 \pm 1.69	30.20 \pm 1.91	23.44 \pm 0.71	12.55 \pm 0.22	10.21 \pm 0.26	4.03 \pm 0.10	2.91 \pm 0.10
(+) CONAN	46.65 \pm 3.36	45.75 \pm 1.92	31.14 \pm 1.88	25.77 \pm 1.18	18.32 \pm 0.42	15.83 \pm 0.34	5.78 \pm 0.17	4.70 \pm 0.14
HIRPG	51.36 \pm 2.59	51.63 \pm 2.49	34.12 \pm 1.27	28.18 \pm 1.32	27.72 \pm 0.30	23.71 \pm 0.39	10.70 \pm 0.19	8.75 \pm 0.13
(+) CONAN (Ours)	55.89 \pm 3.06	55.43 \pm 2.49	38.53\pm1.15	33.73\pm1.82	35.60 \pm 0.31	29.99 \pm 0.11	14.53\pm0.22	12.65\pm0.09
MA	67.10\pm4.07	61.95\pm0.92	27.75 \pm 1.44	20.90 \pm 0.95	51.13\pm0.28	42.95\pm0.15	13.48 \pm 0.09	10.69 \pm 0.07

Table 1: **Quantitative comparison between different name-only baselines on CIL setup.** We follow the ID and OOD domains as described in Tab. 6. MA refers to training a model with manually annotated data.

Method	Bongard-HOI				Bongard-OpenWorld			
	Positive / Negative		Concept Answering		Positive / Negative		Concept Answering	
	$A_{AUC} \uparrow$	$A_{last} \uparrow$	$A_{AUC} \uparrow$	$A_{last} \uparrow$	$A_{AUC} \uparrow$	$A_{last} \uparrow$	$A_{AUC} \uparrow$	$A_{last} \uparrow$
C2C (CoLLAs 2024)	61.53 \pm 3.13	59.58 \pm 2.49	73.88 \pm 3.21	67.40 \pm 3.15	49.75 \pm 0.49	50.39 \pm 0.89	69.56 \pm 3.58	67.56 \pm 1.47
Glide-Syn (ICLR 2023)	54.83 \pm 2.07	55.77 \pm 3.54	67.87 \pm 3.30	59.38 \pm 3.62	-	-	-	-
LE (ICLR 2023)	64.03 \pm 3.10	62.40 \pm 2.58	73.65 \pm 3.60	70.68 \pm 3.80	-	-	-	-
(+) CONAN	65.90 \pm 2.59	65.63 \pm 2.59	74.99 \pm 3.07	72.38 \pm 2.76	-	-	-	-
HIRPG	67.25 \pm 2.61	71.49 \pm 0.42	75.52 \pm 3.17	73.97 \pm 3.11	48.37 \pm 1.17	47.48 \pm 3.47	70.09 \pm 1.92	74.59 \pm 3.11
(+) CONAN (Ours)	70.20\pm3.97	73.18\pm2.40	77.01\pm3.45	75.80\pm1.83	53.68\pm1.18	57.74\pm2.18	73.10\pm3.79	76.77\pm3.81
MA	69.50 \pm 1.84	73.04 \pm 2.71	76.02 \pm 3.85	70.37 \pm 3.87	53.44 \pm 1.91	53.06 \pm 3.45	70.84 \pm 3.44	72.21 \pm 3.75

Table 2: **Quantitative comparison between different name-only baselines on Multi-modal MVCIL setup.**

relevant hard negative concepts based on the specified positive concept, leveraging commonsense priors from large language models (Zhao et al., 2023; Yang et al., 2024). For web-scraped data, since long-context queries (e.g., ‘hard negative images of riding a bike’) often retrieve noisy images, they require negative concepts derived from manually annotated data instead.

Even in the absence of hard negative concepts, GenCL outperforms models trained with both manually annotated and web-scraped data by leveraging the ability of LLMs to generate prompts for hard negative examples and the controllability of T2I generative models through text prompts (Nie et al., 2021). For the prompts we use to select hard negative examples, see Sec. A.4.

Comparison of HIRPG with Diverse Prompt Generation Methods. To evaluate the effectiveness of HIRPG in diverse prompt generation, we compare models trained on data generated from prompts derived by prompt generation baselines (LE, CHB, SC, and CCG). As shown in Tab. 1, HIRPG significantly outperforms the baselines, both with and without the combination of CONAN. We attribute this performance improvement to two key components of the prompts: recurrent prompt generation (RPG), which reduces the overlap between generated prompts, and hierarchical generation (HIG), which addresses the *lost-in-the-middle* challenge (Liu et al., 2024) that arises from solely using RPG. We provide an ablation study of these two components of HIRPG in Sec. A.9. Furthermore, we analyze the Diversity (Naeem et al., 2020) and Recognizability (Fan et al., 2024) of images generated by each prompt generation baseline in Sec. A.5 in the Appendix for the sake of space.

Comparison of CONAN with Data Ensemble Methods. To demonstrate the effectiveness of CONAN, we compare it with existing data ensemble methods (i.e., Moderate, Uncertainty, Glistter, GradMatch, and LCMat), as well as the equal-weight selection (EWS) and No ensembling (i.e., using images generated from a single generative model). We summarize the result in Tab. 3. We employ a CLIP-pretrained ResNet-50 as the backbone network for all baselines. Note that Uncertainty, Glistter, GradMatch, and LCMat require fine-tuning on the full dataset for gradient calculations of the fine-tuned model, even though they use a pre-trained model for initialization. Consequently, for these baselines, we fine-tune the pre-trained ResNet-50 model for 30 epochs using the full dataset

for those baselines. In contrast, Moderate and CONAN do not require fine-tuning; they only need a feature extractor to calculate distances. Despite being training-free, as shown in Tab. 3, CONAN outperforms methods that require fine-tuning with a full dataset, as well as moderate.

We further compare CONAN with various RMD-based ensemble, such as k-highest RMD ensemble, and summarize the results in Sec. A.14 for the space’s sake.

Method	Full Dataset Training	PACS				DomainNet			
		ID		OOD		ID		OOD	
		$A_{AUC} \uparrow$	$A_{last} \uparrow$	$A_{AUC} \uparrow$	$A_{last} \uparrow$	$A_{AUC} \uparrow$	$A_{last} \uparrow$	$A_{AUC} \uparrow$	$A_{last} \uparrow$
No ensembling	✗	51.36±2.59	51.63±2.49	34.12±1.27	28.18±1.32	27.72±0.30	23.71±0.39	10.70±0.19	8.75±0.13
EWS	✗	50.56±2.32	50.03±2.13	34.59±1.41	27.13±3.44	32.38±0.47	26.45±0.35	12.93±0.23	10.92±0.06
Moderate (ICLR 2023)	✗	47.03±3.52	45.34±1.11	35.06±2.03	27.91±2.17	25.57±0.42	20.38±0.16	10.53±0.29	8.17±0.13
CONAN (Ours)	✗	55.89±3.06	55.43±2.49	38.53±1.15	33.73±1.82	34.60±0.31	30.09±0.11	14.53±0.22	12.65±0.09
Uncertainty (ICLR 2020)	✓	39.75±2.10	33.17±3.69	32.99±1.42	25.17±3.01	21.90±0.37	15.70±0.08	10.01±0.23	7.19±0.11
CRAIG (ICML 2020)	✓	53.57±2.43	54.24±2.04	35.54±0.90	32.29±0.96	32.53±0.20	28.44±0.23	13.25±0.15	11.53±0.06
Glister (AAAI 2021)	✓	40.55±2.43	37.75±3.81	34.30±1.66	27.56±1.31	23.16±0.37	16.98±0.35	10.56±0.26	7.60±0.18
GradMatch (ICML 2022)	✓	54.93±3.24	54.06±1.49	35.05±1.70	29.81±1.35	32.53±0.43	28.36±0.41	13.48±0.31	11.74±0.18
Adacore (ICML 2022)	✓	52.06±2.64	48.37±2.80	35.55±2.09	30.36±0.85	32.15±0.55	26.83±0.18	13.62±0.27	11.37±0.04
LCMat (AISTATS 2023)	✓	53.40±2.35	54.60±1.65	35.37±1.62	30.04±0.82	32.38±0.44	28.36±0.32	13.42±0.26	11.76±0.17

Table 3: **Quantitative comparison between data ensemble methods on CIL setup.** EWS refers to the method of selecting and combining generated data from different generative models in equal proportions. No ensembling refers to using a single generative model (*i.e.*, SDXL).

Additionally, we provide a comparison of HIRPG and baselines in the joint training setup in Sec.A.7.

5.3 ABLATION STUDY

We conduct an ablation study on two components of GenCL, *i.e.*, HIRPG and CONAN using the ResNet-18 and ImageNet-1k pretrained ViT-Base models, and summarize the results in Tab. 4 and Tab. 5, respectively. Our observations indicate that both components play a significant role in enhancing not only the ID domain performance but also the OOD domain performance. In the tables, Vanilla GenCL refers to generating 50 different prompts using an LLM without employing RPG or HIG, and using a single T2I generator, *i.e.*, SDXL. We provide the details about Vanilla GenCL in Sec A.9.

Method	PACS				DomainNet			
	ID		OOD		ID		OOD	
	$A_{AUC} \uparrow$	$A_{last} \uparrow$	$A_{AUC} \uparrow$	$A_{last} \uparrow$	$A_{AUC} \uparrow$	$A_{last} \uparrow$	$A_{AUC} \uparrow$	$A_{last} \uparrow$
Vanilla GenCL	47.74±1.52	47.30±2.38	31.66±1.45	25.41±0.66	20.82±0.39	17.19±0.34	7.09±0.21	5.55±0.11
(+) HIRPG	51.36±2.59	51.63±2.49	34.12±1.27	28.18±1.32	27.72±0.30	23.71±0.39	10.70±0.19	8.75±0.13
(+) CONAN	50.02±2.52	45.34±4.25	33.94±1.37	27.30±1.16	28.17±0.35	24.12±0.11	9.76±0.17	8.18±0.15
(+) HIRPG & CONAN (Ours)	55.89±3.06	55.43±2.49	38.53±1.15	33.73±1.82	34.60±0.31	29.99±0.11	14.53±0.22	12.65±0.09

Table 4: **Ablations for proposed components of GenCL.** We use ResNet-18 model.

Method	PACS				DomainNet			
	ID		OOD		ID		OOD	
	$A_{AUC} \uparrow$	$A_{last} \uparrow$	$A_{AUC} \uparrow$	$A_{last} \uparrow$	$A_{AUC} \uparrow$	$A_{last} \uparrow$	$A_{AUC} \uparrow$	$A_{last} \uparrow$
Vanilla GenCL	72.91±1.40	56.85±2.68	40.39±1.67	27.11±2.90	30.96±0.34	22.52±0.46	11.17±0.25	7.78±0.21
(+) HIRPG	78.52±1.90	72.40±2.40	45.46±1.59	36.76±2.35	37.90±0.31	30.37±0.64	15.30±0.19	11.31±0.29
(+) CONAN	77.31±1.58	64.39±2.40	48.01±2.05	35.22±2.64	37.81±0.47	30.15±0.25	14.61±0.29	10.83±0.20
(+) HIRPG & CONAN (Ours)	79.32±1.97	72.46±0.42	53.88±1.57	41.31±2.42	42.73±0.25	36.09±0.50	18.64±0.28	14.68±0.16

Table 5: **Ablations for proposed components of GenCL.** We use ImageNet-1k pretrained ViT-base model.

6 CONCLUSION

Online continual learning represents a practical, real-world-aligned learning paradigm. However, the assumption of having access to well-curated and annotated data in these scenarios hinders its real-world application. To address the challenges arisen from using manually annotated and web-crawled data, we introduce a unified name-only continual learning framework that integrates generators with the continual learner, termed ‘Generative name only Continual Learning’ (**GenCL**).

Within the GenCL framework, we propose an diverse prompt generation method (*i.e.*, HIRPG) and complexity-guided ensembling (*i.e.*, CONAN). Extensive experimental validations demonstrate the performance improvements achieved by both components within the GenCL framework, showcasing its effectiveness in both ID and OOD settings compared to webly-supervised and human supervision.

ETHICS STATEMENT

We propose a better learning scheme for continual learning for realistic learning scenarios. While the authors do not explicitly aim for this, the increasing adoption of deep learning models in real-world contexts with streaming data could potentially raise concerns such as inadvertently introducing biases or discrimination. We note that we are committed to implementing all feasible precautions to avert such consequences, as they are unequivocally contrary to our intentions.

REPRODUCIBILITY STATEMENT

We take reproducibility in deep learning very seriously and highlight some of the contents of the manuscript that might help to reproduce our work. We provide a link in the abstract to access the generated data. Additionally, we will definitely release our implementation of the proposed method in Sec. 4, the data splits and the baselines used in our experiments in Sec. 5

REFERENCES

- Josh Achiam, Steven Adler, Sandhini Agarwal, Lama Ahmad, Ilge Akkaya, Florencia Leoni Aleman, Diogo Almeida, Janko Altschmidt, Sam Altman, Shyamal Anadkat, et al. Gpt-4 technical report. *arXiv preprint arXiv:2303.08774*, 2023.
- Rishabh Agarwal, Avi Singh, Lei M Zhang, Bernd Bohnet, Stephanie Chan, Ankesh Anand, Zaheer Abbas, Azade Nova, John D Co-Reyes, Eric Chu, et al. Many-shot in-context learning. *arXiv preprint arXiv:2404.11018*, 2024.
- Hayri Volkan Agun. Webcollectives: A light regular expression based web content extractor in java. In *SoftwareX*, volume 24, pp. 101569. Elsevier, 2023.
- Guillaume Alain. Understanding intermediate layers using linear classifier probes. *arXiv preprint arXiv:1610.01644*, 2016.
- Shengnan An, Zexiong Ma, Zeqi Lin, Nanning Zheng, and Jian-Guang Lou. Make your llm fully utilize the context. *arXiv preprint arXiv:2404.16811*, 2024.
- Anonymous. Coreset selection for object detection, 2023. URL <https://openreview.net/forum?id=Yyg3DXzaIK>.
- Shekoofeh Azizi, Simon Kornblith, Chitwan Saharia, Mohammad Norouzi, and David J Fleet. Synthetic data from diffusion models improves imagenet classification. *arXiv preprint arXiv:2304.08466*, 2023.
- Max Bain, Arsha Nagrani, Gül Varol, and Andrew Zisserman. Frozen in time: A joint video and image encoder for end-to-end retrieval. In *ICCV*, 2021.
- Simone Balloccu, Patrícia Schmidtová, Mateusz Lango, and Ondřej Dušek. Leak, cheat, repeat: Data contamination and evaluation malpractices in closed-source llms. *arXiv preprint arXiv:2402.03927*, 2024.
- Soumya Banerjee, Vinay K Verma, Avideep Mukherjee, Deepak Gupta, Vinay P Namboodiri, and Piyush Rai. Verse: Virtual-gradient aware streaming lifelong learning with anytime inference. *arXiv preprint arXiv:2309.08227*, 2023.
- Jihwan Bang, Heesu Kim, YoungJoon Yoo, Jung-Woo Ha, and Jonghyun Choi. Rainbow memory: Continual learning with a memory of diverse samples. In *CVPR*, 2021.
- Jihwan Bang, Hyunseo Koh, Seulki Park, Hwanjun Song, Jung-Woo Ha, and Jonghyun Choi. Online continual learning on a contaminated data stream with blurry task boundaries. In *CVPR*, 2022.
- Federico Bianchi, Pratyusha Kalluri, Esin Durmus, Faisal Ladhak, Myra Cheng, Debora Nozza, Tatsunori Hashimoto, Dan Jurafsky, James Zou, and Aylin Caliskan. Easily accessible text-to-image generation amplifies demographic stereotypes at large scale. In *FAccT*, 2023.

- Victor Boutin, Lakshya Singhal, Xavier Thomas, and Thomas Serre. Diversity vs. recognizability: Human-like generalization in one-shot generative models. In *NeurIPS*, 2022.
- Tom Brown, Benjamin Mann, Nick Ryder, Melanie Subbiah, Jared D Kaplan, Prafulla Dhariwal, Arvind Neelakantan, Pranav Shyam, Girish Sastry, Amanda Askell, et al. Language models are few-shot learners. In *NeurIPS*, 2020.
- Lucas Caccia, Jing Xu, Myle Ott, Marcaurelio Ranzato, and Ludovic Denoyer. On anytime learning at macroscale. In *CoLLAs*. PMLR, 2022.
- Aylin Caliskan, Joanna J Bryson, and Arvind Narayanan. Semantics derived automatically from language corpora contain human-like biases. *Science*, 356(6334):183–186, 2017.
- Tânia Carvalho, Nuno Moniz, Luís Antunes, and Nitesh Chawla. Differentially-private data synthetisation for efficient re-identification risk control. *arXiv preprint arXiv:2212.00484*, 2022.
- Muxi Chen, Yi Liu, Jian Yi, Changran Xu, Qiuxia Lai, Hongliang Wang, Tsung-Yi Ho, and Qiang Xu. Evaluating text-to-image generative models: An empirical study on human image synthesis. *arXiv preprint arXiv:2403.05125*, 2024.
- Qingrong Chen, Chong Xiang, Minhui Xue, Bo Li, Nikita Borisov, Dali Kaarfar, and Haojin Zhu. Differentially private data generative models. *arXiv preprint arXiv:1812.02274*, 2018.
- Xiao Chen, Thomas Navidi, Stefano Ermon, and Ram Rajagopal. Distributed generation of privacy preserving data with user customization. *arXiv preprint arXiv:1904.09415*, 2019.
- Yunzhuo Chen, Naveed Akhtar, Nur Al Hasan Haldar, and Ajmal Mian. On quantifying and improving realism of images generated with diffusion. *arXiv preprint arXiv:2309.14756*, 2023a.
- Zijian Chen, Wei Sun, Haoning Wu, Zicheng Zhang, Jun Jia, Xiongkuo Min, Guangtao Zhai, and Wenjun Zhang. Exploring the naturalness of ai-generated images. *arXiv preprint arXiv:2312.05476*, 2023b.
- Yew Ken Chia, Guizhen Chen, Luu Anh Tuan, Soujanya Poria, and Lidong Bing. Contrastive chain-of-thought prompting. *arXiv preprint arXiv:2311.09277*, 2023.
- C Coleman, C Yeh, S Musmann, B Mirzasoleiman, P Bailis, P Liang, J Leskovec, and M Zaharia. Selection via proxy: Efficient data selection for deep learning. In *ICLR*, 2020.
- Ekin D Cubuk, Barret Zoph, Jonathon Shlens, and Quoc V Le. Randaugment: Practical automated data augmentation with a reduced search space. In *CVPRW*, 2020.
- Peng Cui, Dan Zhang, Zhijie Deng, Yinpeng Dong, and Jun Zhu. Learning sample difficulty from pre-trained models for reliable prediction. In *NeurIPS*, 2023.
- Jasper Dekoninck, Mark Niklas Müller, Maximilian Baader, Marc Fischer, and Martin Vechev. Evading data contamination detection for language models is (too) easy. *arXiv preprint arXiv:2402.02823*, 2024.
- Jia Deng, Wei Dong, Richard Socher, Li-Jia Li, Kai Li, and Li Fei-Fei. Imagenet: A large-scale hierarchical image database. In *CVPR*, 2009.
- Ming Ding, Zhuoyi Yang, Wenyi Hong, Wendi Zheng, Chang Zhou, Da Yin, Junyang Lin, Xu Zou, Zhou Shao, Hongxia Yang, et al. Cogview: Mastering text-to-image generation via transformers. In *NeurIPS*, 2021.
- Ming Ding, Wendi Zheng, Wenyi Hong, and Jie Tang. Cogview2: Faster and better text-to-image generation via hierarchical transformers. In *NeurIPS*, 2022.
- Xiaoyi Dong, Pan Zhang, Yuhang Zang, Yuhang Cao, Bin Wang, Linke Ouyang, Xilin Wei, Songyang Zhang, Haodong Duan, Maosong Cao, et al. Internlm-xcomposer2: Mastering free-form text-image composition and comprehension in vision-language large model. *arXiv preprint arXiv:2401.16420*, 2024.

- A. Dosovitskiy and T. Brox. Inverting visual representations with convolutional networks. In *CVPR*, 2016.
- Ethan R Elenberg, Rajiv Khanna, Alexandros G Dimakis, and Sahand Negahban. Restricted strong convexity implies weak submodularity. *arXiv preprint arXiv:1612.00804*, 2016.
- Patrick Esser, Sumith Kulal, Andreas Blattmann, Rahim Entezari, Jonas Müller, Harry Saini, Yam Levi, Dominik Lorenz, Axel Sauer, Frederic Boesel, et al. Scaling rectified flow transformers for high-resolution image synthesis. In *ICML*, 2024.
- Lijie Fan, Kaifeng Chen, Dilip Krishnan, Dina Katabi, Phillip Isola, and Yonglong Tian. Scaling laws of synthetic images for model training... for now. In *CVPR*, 2024.
- Jens Foerderer. Should we trust web-scraped data? *arXiv preprint arXiv:2308.02231*, 2023.
- Kathleen C Fraser, Svetlana Kiritchenko, and Isar Nejadgholi. Diversity is not a one-way street: Pilot study on ethical interventions for racial bias in text-to-image systems. In *ICCV*, 2023.
- Leo Gao, Stella Biderman, Sid Black, Laurence Golding, Travis Hoppe, Charles Foster, Jason Phang, Horace He, Anish Thite, Noa Nabeshima, et al. The pile: An 800gb dataset of diverse text for language modeling. *arXiv preprint arXiv:2101.00027*, 2020.
- Gabriele Graffieti, Davide Maltoni, Lorenzo Pellegrini, and Vincenzo Lomonaco. Generative negative replay for continual learning. *Neural Networks*, 2023.
- Jonathan L Gross, Jay Yellen, and Mark Anderson. *Graph theory and its applications*. Chapman and Hall/CRC, 2018.
- Jiatao Gu, Qingzhe Gao, Shuangfei Zhai, Baoquan Chen, Lingjie Liu, and Josh Susskind. Learning controllable 3d diffusion models from single-view images. *arXiv preprint arXiv:2304.06700*, 2023.
- Ziyu Guo, Renrui Zhang, Longtian Qiu, Xianzheng Ma, Xupeng Miao, Xuming He, and Bin Cui. Calip: Zero-shot enhancement of clip with parameter-free attention. In *AAAI*, 2023.
- Alon Halevy, Flip Korn, Natalya F Noy, Christopher Olston, Neoklis Polyzotis, Sudip Roy, and Steven Euijong Whang. Goods: Organizing google’s datasets. In *SIGMOD*, 2016.
- Hasan Abed Al Kader Hammoud, Hani Itani, Fabio Pizzati, Philip Torr, Adel Bibi, and Bernard Ghanem. Synthclip: Are we ready for a fully synthetic clip training? *arXiv preprint arXiv:2402.01832*, 2024.
- Jiyeon Han, Hwanil Choi, Yunje Choi, Junho Kim, Jung-Woo Ha, and Jaesik Choi. Rarity score: A new metric to evaluate the uncommonness of synthesized images. *arXiv preprint arXiv:2206.08549*, 2022.
- Md Yousuf Harun, Jhair Gallardo, and Christopher Kanan. Grasp: A rehearsal policy for efficient online continual learning. *arXiv preprint arXiv:2308.13646*, 2023.
- Jinghan He, Haiyun Guo, Ming Tang, and Jinqiao Wang. Continual instruction tuning for large multimodal models. *arXiv preprint arXiv:2311.16206*, 2023a.
- Kaiming He, Xiangyu Zhang, Shaoqing Ren, and Jian Sun. Deep residual learning for image recognition. In *CVPR*, 2016.
- Ruifei He, Shuyang Sun, Xin Yu, Chuhui Xue, Wenqing Zhang, Philip Torr, Song Bai, and Xiaojuan Qi. Is synthetic data from generative models ready for image recognition? In *ICLR*, 2023b.
- Danny Hernandez, Jared Kaplan, Tom Henighan, and Sam McCandlish. Scaling laws for transfer. *arXiv preprint arXiv:2102.01293*, 2021.
- Jordan Hoffmann, Sebastian Borgeaud, Arthur Mensch, Elena Buchatskaya, Trevor Cai, Eliza Rutherford, Diego de Las Casas, Lisa Anne Hendricks, Johannes Welbl, Aidan Clark, et al. Training compute-optimal large language models. *arXiv preprint arXiv:2203.15556*, 2022.

- Edward J Hu, Yelong Shen, Phillip Wallis, Zeyuan Allen-Zhu, Yanzhi Li, Shean Wang, Lu Wang, and Weizhu Chen. Lora: Low-rank adaptation of large language models. *arXiv preprint arXiv:2106.09685*, 2021.
- Jaehui Hwang, Junghyuk Lee, and Jong-Seok Lee. Anomaly score: Evaluating generative models and individual generated images based on complexity and vulnerability. *arXiv preprint arXiv:2312.10634*, 2023.
- Huaizu Jiang, Xiaojian Ma, Weili Nie, Zhiding Yu, Yuke Zhu, and Anima Anandkumar. Bongard-hoi: Benchmarking few-shot visual reasoning for human-object interactions. In *CVPR*, 2022.
- Maxwell Jones, Sheng-Yu Wang, Nupur Kumari, David Bau, and Jun-Yan Zhu. Customizing text-to-image models with a single image pair. *arXiv preprint arXiv:2405.01536*, 2024.
- Cheng Ju, Aurélien Bibaut, and Mark van der Laan. The relative performance of ensemble methods with deep convolutional neural networks for image classification. *Journal of applied statistics*, 45(15):2800–2818, 2018.
- Sina Khajehabdollahi, Georg Martius, and Anna Levina. Assessing aesthetics of generated abstract images using correlation structure. In *SSCI*, 2019.
- Mehtab Khan and Alex Hanna. The legality of computer vision datasets. *Under review*, 2020.
- Krishnateja Killamsetty, Sivasubramanian Durga, Ganesh Ramakrishnan, Abir De, and Rishabh Iyer. Grad-match: Gradient matching based data subset selection for efficient deep model training. In *ICML*, 2021a.
- Krishnateja Killamsetty, Durga Sivasubramanian, Ganesh Ramakrishnan, and Rishabh Iyer. Glisten: Generalization based data subset selection for efficient and robust learning. In *AAAI*, 2021b.
- Byeonghwi Kim, Minhyuk Seo, and Jonghyun Choi. Online continual learning for interactive instruction following agents. In *ICLR*, 2024a.
- Chris Dongjoo Kim, Jinseo Jeong, Sangwoo Moon, and Gunhee Kim. Continual learning on noisy data streams via self-purified replay. In *ICCV*, 2021.
- Jang-Hyun Kim, Jinuk Kim, Seong Joon Oh, Sangdoo Yun, Hwanjun Song, Joonhyun Jeong, Jung-Woo Ha, and Hyun Oh Song. Dataset condensation via efficient synthetic-data parameterization. In *ICML*, 2022.
- Pum Jun Kim, Yoojin Jang, Jisu Kim, and Jaejun Yoo. Topp&r: Robust support estimation approach for evaluating fidelity and diversity in generative models. In *NeurIPS*, 2024b.
- Denis Kocetkov, Raymond Li, Loubna Ben Allal, Jia Li, Chenghao Mou, Carlos Muñoz Ferrandis, Yacine Jernite, Margaret Mitchell, Sean Hughes, Thomas Wolf, et al. The stack: 3 tb of permissively licensed source code. *arXiv preprint arXiv:2211.15533*, 2022.
- Hyunseo Koh, Dahyun Kim, Jung-Woo Ha, and Jonghyun Choi. Online continual learning on class incremental blurry task configuration with anytime inference. In *ICLR*, 2021.
- Hyunseo Koh, Minhyuk Seo, Jihwan Bang, Hwanjun Song, Deokki Hong, Seulki Park, Jung-Woo Ha, and Jonghyun Choi. Online boundary-free continual learning by scheduled data prior. In *ICLR*, 2023.
- Jędrzej Kozal, Jan Wasilewski, Bartosz Krawczyk, and Michał Woźniak. Continual learning with weight interpolation. *arXiv preprint arXiv:2404.04002*, 2024.
- Alex Krizhevsky, Geoffrey Hinton, et al. Learning multiple layers of features from tiny images. 2009.
- Alexander C Li, Mihir Prabhudesai, Shivam Duggal, Ellis Brown, and Deepak Pathak. Your diffusion model is secretly a zero-shot classifier. In *ICCV*, 2023.
- Tianle Li, Ge Zhang, Quy Duc Do, Xiang Yue, and Wenhui Chen. Long-context llms struggle with long in-context learning. *arXiv preprint arXiv:2404.02060*, 2024.

- Yucheng Li. An open source data contamination report for llama series models. *arXiv preprint arXiv:2310.17589*, 2023.
- Jian Liang, Chenfei Wu, Xiaowei Hu, Zhe Gan, Jianfeng Wang, Lijuan Wang, Zicheng Liu, Yuejian Fang, and Nan Duan. Nuwa-infinity: Autoregressive over autoregressive generation for infinite visual synthesis. In *NeurIPS*, 2022.
- Bill Yuchen Lin, Wangchunshu Zhou, Ming Shen, Pei Zhou, Chandra Bhagavatula, Yejin Choi, and Xiang Ren. CommonGen: A constrained text generation challenge for generative commonsense reasoning. *arXiv preprint arXiv:1911.03705*, 2019.
- Bill Yuchen Lin, Wangchunshu Zhou, Ming Shen, Pei Zhou, Chandra Bhagavatula, Yejin Choi, and Xiang Ren. CommonGen: A constrained text generation challenge for generative commonsense reasoning. In *EMNLP*, 2020.
- Guisheng Liu, Yi Li, Zhengcong Fei, Haiyan Fu, Xiangyang Luo, and Yanqing Guo. Prefix-diffusion: A lightweight diffusion model for diverse image captioning. *arXiv preprint arXiv:2309.04965*, 2023a.
- Haotian Liu, Chunyuan Li, Qingyang Wu, and Yong Jae Lee. Visual instruction tuning. In *NeurIPS*, 2023b.
- Nelson F Liu, Kevin Lin, John Hewitt, Ashwin Paranjape, Michele Bevilacqua, Fabio Petroni, and Percy Liang. Lost in the middle: How language models use long contexts. *Transactions of the Association for Computational Linguistics*, 12:157–173, 2024.
- Xingchao Liu, Chengyue Gong, et al. Flow straight and fast: Learning to generate and transfer data with rectified flow. In *ICLR*, 2023c.
- Alejandro López-Cifuentes, Marcos Escudero-Vinolo, Jesús Bescós, and Álvaro García-Martín. Semantic-aware scene recognition. *Pattern Recognition*, 102:107256, 2020.
- Nils Lukas, Ahmed Salem, Robert Sim, Shruti Tople, Lukas Wutschitz, and Santiago Zanella-Béguelin. Analyzing leakage of personally identifiable information in language models. *arXiv preprint arXiv:2302.00539*, 2023.
- Divyam Madaan, Jaehong Yoon, Yuanchun Li, Yunxin Liu, and Sung Ju Hwang. Representational continuity for unsupervised continual learning. *arXiv preprint arXiv:2110.06976*, 2021.
- Prasanta Chandra Mahalanobis. On the generalized distance in statistics. *Sankhyā: The Indian Journal of Statistics, Series A (2008-)*, 80:S1–S7, 2018.
- Sachit Menon and Carl Vondrick. Visual classification via description from large language models. In *ICLR*, 2023.
- George A Miller. Wordnet: a lexical database for english. *Communications of the ACM*, 38(11): 39–41, 1995.
- Baharan Mirzasoleiman, Jeff Bilmes, and Jure Leskovec. Coresets for data-efficient training of machine learning models. In *ICML*. PMLR, 2020.
- Madhumita Murgia and Max Harlow. Who’s using your face? the ugly truth about facial recognition. *Financial Times*, 19:1, 2019.
- Muhammad Ferjad Naeem, Seong Joon Oh, Youngjung Uh, Yunje Choi, and Jaejun Yoo. Reliable fidelity and diversity metrics for generative models. In *ICML*. PMLR, 2020.
- Behnam Neyshabur, Hanie Sedghi, and Chiyuan Zhang. What is being transferred in transfer learning? In *NeurIPS*, 2020.
- Alex Nichol, Prafulla Dhariwal, Aditya Ramesh, Pranav Shyam, Pamela Mishkin, Bob McGrew, Ilya Sutskever, and Mark Chen. Glide: Towards photorealistic image generation and editing with text-guided diffusion models. *arXiv preprint arXiv:2112.10741*, 2021.

- Weili Nie, Arash Vahdat, and Anima Anandkumar. Controllable and compositional generation with latent-space energy-based models. In *NeurIPS*, 2021.
- Liz O’Sullivan. Don’t steal data. In *NeurIPS*, 2020.
- Ben Packer, M Mitchell, Mario Guajardo-Céspedes, and Yoni Halpern. Text embeddings contain bias. here’s why that matters. 2018.
- German I Parisi, Ronald Kemker, Jose L Part, Christopher Kanan, and Stefan Wermter. Continual lifelong learning with neural networks: A review. In *Neural networks*, 2019.
- David Patterson, Joseph Gonzalez, Quoc Le, Chen Liang, Lluís-Miquel Munguia, Daniel Rothchild, David So, Maud Texier, and Jeff Dean. Carbon emissions and large neural network training. *arXiv preprint arXiv:2104.10350*, 2021.
- Mansheej Paul, Surya Ganguli, and Gintare Karolina Dziugaite. Deep learning on a data diet: Finding important examples early in training. In *NeurIPS*, 2021.
- William Peebles and Saining Xie. Scalable diffusion models with transformers. In *ICCV*, 2023.
- Lorenzo Pellegrini, Gabriele Graffieti, Vincenzo Lomonaco, and Davide Maltoni. Latent replay for real-time continual learning. In *IROS*. IEEE, 2020.
- Dustin Podell, Zion English, Kyle Lacey, Andreas Blattmann, Tim Dockhorn, Jonas Müller, Joe Penna, and Robin Rombach. Sdxl: Improving latent diffusion models for high-resolution image synthesis. *arXiv preprint arXiv:2307.01952*, 2023.
- Omead Pooladzandi, David Davini, and Baharan Mirzasoleiman. Adaptive second order coresets for data-efficient machine learning. In *ICML*. PMLR, 2022.
- Ameya Prabhu, Philip HS Torr, and Puneet K Dokania. Gdumb: A simple approach that questions our progress in continual learning. In *ECCV*, 2020.
- Ameya Prabhu, Hasan Abed Al Kader Hammoud, Puneet K Dokania, Philip HS Torr, Ser-Nam Lim, Bernard Ghanem, and Adel Bibi. Computationally budgeted continual learning: What does matter? In *CVPR*, 2023.
- Ameya Prabhu, Hasan Abed Al Kader Hammoud, Ser-Nam Lim, Bernard Ghanem, Philip HS Torr, and Adel Bibi. From categories to classifier: Name-only continual learning by exploring the web. In *CoLLAs*, 2024.
- Sarah Pratt, Ian Covert, Rosanne Liu, and Ali Farhadi. What does a platypus look like? generating customized prompts for zero-shot image classification. In *ICCV*, 2023.
- Qi Qian, Yuanhong Xu, and Juhua Hu. Intra-modal proxy learning for zero-shot visual categorization with clip. *Advances in Neural Information Processing Systems*, 36, 2024.
- Jenny Quang. Does training ai violate copyright law? *Berkeley Tech. LJ*, 36:1407, 2021.
- Alec Radford, Jong Wook Kim, Chris Hallacy, Aditya Ramesh, Gabriel Goh, Sandhini Agarwal, Girish Sastry, Amanda Askell, Pamela Mishkin, Jack Clark, et al. Learning transferable visual models from natural language supervision. In *ICML*. PMLR, 2021.
- Colin Raffel, Noam Shazeer, Adam Roberts, Katherine Lee, Sharan Narang, Michael Matena, Yanqi Zhou, Wei Li, and Peter J Liu. Exploring the limits of transfer learning with a unified text-to-text transformer. *JMLR*, 2020.
- Vinay Venkatesh Ramasesh, Aitor Lewkowycz, and Ethan Dyer. Effect of scale on catastrophic forgetting in neural networks. In *ICLR*, 2022. URL https://openreview.net/forum?id=GhVS8_yPeEa.
- Aditya Ramesh, Prafulla Dhariwal, Alex Nichol, Casey Chu, and Mark Chen. Hierarchical text-conditional image generation with clip latents. *arXiv preprint arXiv:2204.06125*, 2022.

- Jie Ren, Stanislav Fort, Jeremiah Liu, Abhijit Guha Roy, Shreyas Padhy, and Balaji Lakshminarayanan. A simple fix to mahalanobis distance for improving near-ood detection. In *ICML Workshop*, 2021.
- Stephen Robertson. Understanding inverse document frequency: on theoretical arguments for idf. *Journal of documentation*, 60(5):503–520, 2004.
- David Rolnick, Arun Ahuja, Jonathan Schwarz, Timothy Lillicrap, and Gregory Wayne. Experience replay for continual learning. In *NeurIPS*, 2019.
- Olaf Ronneberger, Philipp Fischer, and Thomas Brox. U-net: Convolutional networks for biomedical image segmentation. In *MICCAI*, 2015.
- Olga Russakovsky, Jia Deng, Hao Su, Jonathan Krause, Sanjeev Satheesh, Sean Ma, Zhiheng Huang, Andrej Karpathy, Aditya Khosla, Michael Bernstein, et al. Imagenet large scale visual recognition challenge. In *IJCV*, 2015.
- Seyedmorteza Sadat, Jakob Buhmann, Derek Bradely, Otmar Hilliges, and Romann M Weber. Cads: Unleashing the diversity of diffusion models through condition-annealed sampling. *arXiv preprint arXiv:2310.17347*, 2023.
- Mert Bülent Sariyıldız, Karteek Alahari, Diane Larlus, and Yannis Kalantidis. Fake it till you make it: Learning transferable representations from synthetic imagenet clones. In *CVPR*, 2023.
- Ryoma Sato. Active learning from the web. In *WWW*, 2023.
- Christoph Schuhmann, Romain Beaumont, Richard Vencu, Cade Gordon, Ross Wightman, Mehdi Cherti, Theo Coombes, Aarush Katta, Clayton Mullis, Mitchell Wortsman, et al. Laion-5b: An open large-scale dataset for training next generation image-text models. In *NeurIPS*, 2022.
- Roy Schwartz, Jesse Dodge, Noah A Smith, and Oren Etzioni. Green ai. *Communications of the ACM*, 63(12):54–63, 2020.
- Minhyuk Seo, Hyunseo Koh, and Jonghyun Choi. Budgeted online continual learning by adaptive layer freezing and frequency-based sampling. In *OpenReview*, 2024a. URL <https://openreview.net/forum?id=3klVRLhK7w>.
- Minhyuk Seo, Hyunseo Koh, Wonje Jeung, Minjae Lee, San Kim, Hankook Lee, Sungjun Cho, Sungik Choi, Hyunwoo Kim, and Jonghyun Choi. Learning equi-angular representations for online continual learning. In *CVPR*, 2024b.
- Mohsen Shahhosseini, Guiping Hu, and Hieu Pham. Optimizing ensemble weights and hyperparameters of machine learning models for regression problems. *Machine Learning with Applications*, 7: 100251, 2022.
- Murray Shanahan, Christos Kaplanis, and Jovana Mitrović. Encoders and ensembles for task-free continual learning. *arXiv preprint arXiv:2105.13327*, 2021.
- Or Sharir, Barak Peleg, and Yoav Shoham. The cost of training nlp models: A concise overview. *arXiv preprint arXiv:2004.08900*, 2020.
- Yongxin Shi, Dezhi Peng, Wenhui Liao, Zening Lin, Xinhong Chen, Chongyu Liu, Yuyi Zhang, and Lianwen Jin. Exploring ocr capabilities of gpt-4v (ision): A quantitative and in-depth evaluation. *arXiv preprint arXiv:2310.16809*, 2023.
- Hanul Shin, Jung Kwon Lee, Jaehong Kim, and Jiwon Kim. Continual learning with deep generative replay. In *NeurIPS*, 2017.
- Seungjae Shin, Heesun Bae, Donghyeok Shin, Weonyoung Joo, and Il-Chul Moon. Loss-curvature matching for dataset selection and condensation. In *AISTATS*, 2023.
- Aleksandar Shtedritski, Christian Rupprecht, and Andrea Vedaldi. What does clip know about a red circle? visual prompt engineering for vlms. *arXiv preprint arXiv:2304.06712*, 2023.
- Adrians Skapars, Edoardo Manino, Youcheng Sun, and Lucas C Cordeiro. Was it slander? towards exact inversion of generative language models. *arXiv preprint arXiv:2407.11059*, 2024.

- Olivia Solon. Facial recognition’s ‘dirty little secret’: Millions of online photos scraped without consent. In *NBC News*, volume 12, 2019.
- Gowthami Somepalli, Anubhav Gupta, Kamal Gupta, Shramay Palta, Micah Goldblum, Jonas Geiping, Abhinav Shrivastava, and Tom Goldstein. Measuring style similarity in diffusion models. *arXiv preprint arXiv:2404.01292*, 2024.
- Yifan Song, Guoyin Wang, Sujian Li, and Bill Yuchen Lin. The good, the bad, and the greedy: Evaluation of llms should not ignore non-determinism. *arXiv preprint arXiv:2407.10457*, 2024.
- Hongjin Su, Jungo Kasai, Chen Henry Wu, Weijia Shi, Tianlu Wang, Jiayi Xin, Rui Zhang, Mari Ostendorf, Luke Zettlemoyer, Noah A Smith, et al. Selective annotation makes language models better few-shot learners. *arXiv preprint arXiv:2209.01975*, 2022.
- Nishant Subramani, Sasha Luccioni, Jesse Dodge, and Margaret Mitchell. Detecting personal information in training corpora: an analysis. In *TrustNLP*, 2023.
- Xiaoxiao Sun, Liang Zheng, Yu-Kun Lai, and Jufeng Yang. Learning from web data: the benefit of unsupervised object localization. *arXiv preprint arXiv:1812.09232*, 2018.
- Xiaoxiao Sun, Xingjian Leng, Zijian Wang, Yang Yang, Zi Huang, and Liang Zheng. Cifar-10-warehouse: Broad and more realistic testbeds in model generalization analysis. In *ICLR*, 2024.
- Jiapeng Tang, Yinyu Nie, Lev Markhasin, Angela Dai, Justus Thies, and Matthias Nießner. Diffuscene: Scene graph denoising diffusion probabilistic model for generative indoor scene synthesis. *arXiv preprint arXiv:2303.14207*, 2023.
- Kevin Thandiackal, Tiziano Portenier, Andrea Giovannini, Maria Gabrani, and Orcun Goksel. Generative feature-driven image replay for continual learning. *arXiv*, 2021.
- Bart Thomee, David A Shamma, Gerald Friedland, Benjamin Elizalde, Karl Ni, Douglas Poland, Damian Borth, and Li-Jia Li. Yfcc100m: The new data in multimedia research. *Communications of the ACM*, 2016.
- Yonglong Tian, Lijie Fan, Kaifeng Chen, Dina Katabi, Dilip Krishnan, and Phillip Isola. Learning vision from models rivals learning vision from data. In *CVPR*, 2024a.
- Yonglong Tian, Lijie Fan, Phillip Isola, Huiwen Chang, and Dilip Krishnan. Stablerep: Synthetic images from text-to-image models make strong visual representation learners. In *NeurIPS*, 2024b.
- Vishaal Udandarao, Ankush Gupta, and Samuel Albanie. Sus-x: Training-free name-only transfer of vision-language models. In *ICCV*, 2023.
- Gido M Van de Ven and Andreas S Tolias. Generative replay with feedback connections as a general strategy for continual learning. *arXiv*, 2018.
- Gido M Van de Ven, Hava T Siegelmann, and Andreas S Tolias. Brain-inspired replay for continual learning with artificial neural networks. *Nature communications*, 2020.
- Elen Vardanyan, Arshak Minasyan, Sona Hunanyan, Tigran Galstyan, and Arnak Dalalyan. Guaranteed optimal generative modeling with maximum deviation from the empirical distribution. In *ICML*, 2024.
- Ramakrishna Vedantam, C Lawrence Zitnick, and Devi Parikh. Cider: Consensus-based image description evaluation. In *CVPR*, 2015.
- Zifeng Wang, Zizhao Zhang, Chen-Yu Lee, Han Zhang, Ruoxi Sun, Xiaoqi Ren, Guolong Su, Vincent Perot, Jennifer Dy, and Tomas Pfister. Learning to prompt for continual learning. In *CVPR*, 2022.
- Emily Wenger, Xiuyu Li, Ben Y Zhao, and Vitaly Shmatikov. Data isotopes for data provenance in dnns. *arXiv preprint arXiv:2208.13893*, 2022.
- Rujie Wu, Xiaojian Ma, Qing Li, Wei Wang, Zhenliang Zhang, Song-Chun Zhu, and Yizhou Wang. Bongard-openworld: Few-shot reasoning for free-form visual concepts in the real world. In *ICLR*, 2024a.

- Tongtong Wu, Linhao Luo, Yuan-Fang Li, Shirui Pan, Thuy-Trang Vu, and Gholamreza Haffari. Continual learning for large language models: A survey. *arXiv preprint arXiv:2402.01364*, 2024b.
- Yiqi Wu, Xiaodan Hu, Ziming Fu, Siling Zhou, and Jiangong Li. Gpt-4o: Visual perception performance of multimodal large language models in piglet activity understanding. *arXiv preprint arXiv:2406.09781*, 2024c.
- Xiaobo Xia, Jiale Liu, Jun Yu, Xu Shen, Bo Han, and Tongliang Liu. Moderate coreset: A universal method of data selection for real-world data-efficient deep learning. In *ICLR*, 2023.
- Weijie Xu, Jinjin Zhao, Francis Iannacci, and Bo Wang. Ffpdg: Fast, fair and private data generation. *arXiv preprint arXiv:2307.00161*, 2023.
- Zhipeng Xu, Zhenghao Liu, Yukun Yan, Zhiyuan Liu, Chenyan Xiong, and Ge Yu. Cleaner pretraining corpus curation with neural web scraping. In *ACL*, 2024.
- Linting Xue, Noah Constant, Adam Roberts, Mihir Kale, Rami Al-Rfou, Aditya Siddhant, Aditya Barua, and Colin Raffel. mt5: A massively multilingual pre-trained text-to-text transformer. In *NACCL*, 2020.
- S Yang, Z Xie, H Peng, M Xu, M Sun, and P Li. Dataset pruning: Reducing training data by examining generalization influence. *arxiv. arXiv preprint arXiv:2205.09329*, 2022a.
- Shuo Yang, Peize Sun, Yi Jiang, Xiaobo Xia, Ruiheng Zhang, Zehuan Yuan, Changhu Wang, Ping Luo, and Min Xu. Objects in semantic topology. In *ICLR*, 2022b.
- Suorong Yang, Hongchao Yang, Suhan Guo, Furao Shen, and Jian Zhao. Not all data matters: An end-to-end adaptive dataset pruning framework for enhancing model performance and efficiency. *arXiv preprint arXiv:2312.05599*, 2023.
- Yue Yang, Fan-Yun Sun, Luca Weihs, Eli VanderBilt, Alvaro Herrasti, Winson Han, Jiajun Wu, Nick Haber, Ranjay Krishna, Lingjie Liu, et al. Holodeck: Language guided generation of 3d embodied ai environments. In *CVPR*, 2024.
- Qinghao Ye, Haiyang Xu, Guohai Xu, Jiabo Ye, Ming Yan, Yiyang Zhou, Junyang Wang, Anwen Hu, Pengcheng Shi, Yaya Shi, et al. mplug-owl: Modularization empowers large language models with multimodality. *arXiv preprint arXiv:2304.14178*, 2023.
- Jason Yoo, Yunpeng Liu, Frank Wood, and Geoff Pleiss. Layerwise proximal replay: A proximal point method for online continual learning. *arXiv preprint arXiv:2402.09542*, 2024.
- Dawen Zhang, Boming Xia, Yue Liu, Xiwei Xu, Thong Hoang, Zhenchang Xing, Mark Staples, Qinghua Lu, and Liming Zhu. Tag your fish in the broken net: A responsible web framework for protecting online privacy and copyright. *arXiv preprint arXiv:2310.07915*, 2023a.
- Tianhui Zhang, Bei Peng, and Danushka Bollegala. Improving diversity of commonsense generation by large language models via in-context learning. *arXiv preprint arXiv:2404.16807*, 2024a.
- Tianjun Zhang, Aman Madaan, Luyu Gao, Steven Zheng, Swaroop Mishra, Yiming Yang, Niket Tandon, and Uri Alon. In-context principle learning from mistakes, 2024b.
- Tiantian Zhang, Kevin Zehua Shen, Zichuan Lin, Bo Yuan, Xueqian Wang, Xiu Li, and Deheng Ye. Replay-enhanced continual reinforcement learning. *arXiv preprint arXiv:2311.11557*, 2023b.
- Xingxuan Zhang, Yue He, Renzhe Xu, Han Yu, Zheyang Shen, and Peng Cui. Nico++: Towards better benchmarking for domain generalization. In *CVPR*, 2023c.
- Yifan Zhang, Daquan Zhou, Bryan Hooi, Kai Wang, and Jiashi Feng. Expanding small-scale datasets with guided imagination. In *NeurIPS*, 2024c.
- Bo Zhao, Konda Reddy Mopuri, and Hakan Bilen. Dataset condensation with gradient matching. In *ICLR*, 2021.
- Zirui Zhao, Wee Sun Lee, and David Hsu. Large language models as commonsense knowledge for large-scale task planning. In *NeurIPS*, 2023.

Kaiyang Zhou, Yongxin Yang, Timothy Hospedales, and Tao Xiang. Deep domain-adversarial image generation for domain generalisation. In *AAAI*, 2020.

Wanrong Zhu, Jack Hessel, Anas Awadalla, Samir Yitzhak Gadre, Jesse Dodge, Alex Fang, Youngjae Yu, Ludwig Schmidt, William Yang Wang, and Yejin Choi. Multimodal c4: An open, billion-scale corpus of images interleaved with text. In *NeurIPS*, 2024.

A APPENDIX

A.1 DETAILS ABOUT VISUAL-CONCEPT INCREMENTAL LEARNING SETUP

Beyond CIL setups, we also assess GenCL in multimodal tasks, such as context-dependent visual reasoning tasks, focusing on Bongard-HOI (Jiang et al., 2022) and Bongard-OpenWorld (Wu et al., 2024a). These benchmarks are based on two desirable characteristics of classical Bongard problems: (1) few-shot concept learning and (2) context-dependent reasoning. The former refers to the ability to induce visual concepts from a small number of examples, while the latter indicates that the label of a query image may vary depending on the given context (*i.e.*, positive and negative support set). Specifically, as shown in Fig. 4 and Fig. 5, given a positive support set and a negative support set for a particular concept (*e.g.*, "ride a bike"), we consider two types of tasks that address the following queries: (1) *What is the concept exclusively depicted by the positive support set?* and (2) *Given a query image, does the query image belong to the positive or negative support set?* We refer to these tasks as CA (Concept Answering) and P/N, respectively. In addition, we provide a detailed description of each visual concept reasoning benchmark.

Bongard-HOI (Jiang et al., 2022). Bongard-HOI denotes a concept $c = \langle a, o \rangle$ as a visual relationship tuple, where a, o are the class labels of action and object, respectively. Following Bongard’s characteristic, there are positive support set \mathcal{I}_p and negative support set \mathcal{I}_n , where \mathcal{I}_p and \mathcal{I}_n have different concepts. Specifically, if the concept of \mathcal{I}_p is $\langle a, c \rangle$, \mathcal{I}_n is composed of data with concept $c' = \langle \bar{a}, o \rangle$, where $\bar{a} \neq a$. As a result, images from both \mathcal{I}_n and \mathcal{I}_p contain the same categories of objects, with the only difference being the action labels, making it impossible to trivially distinguish positive images from negative ones through visual recognition of object categories alone (*i.e.*, hard negative examples). We provide examples of Bongard-HOI-CA & Bongard-HOI-P/N (Jiang et al., 2022) in Fig. 4.

Bongard-OpenWorld (Wu et al., 2024a). In contrast to Bongard-HOI, which has a structured concept c represented as (action, object), Bongard-OpenWorld utilizes a free-form sentence as c to describe the content depicted by all images in the positive set \mathcal{I}_p exclusively. Specifically, concepts are obtained by the annotators, who are instructed to write visual concepts by following a predefined set of categories. We provide examples of Bongard-OpenWorld-CA & Bongard-OpenWorld-P/N (Wu et al., 2024a) in Fig. 5.

Note that since the input consists of both text queries and images (*i.e.*, support sets and a query image) and outputs are sentences, we use multimodal large language models (MLLMs), such as LLaVA (Liu et al., 2023b), which connects a vision encoder with an LLM for general-purpose visual and language understanding. For further implementation details, such as the prompts we use, see Sec. A.3.

A.2 DETAILS ABOUT EXPERIMENT SETUP

To set a domain generalization benchmarks (*i.e.*, PACS (Zhou et al., 2020), DomainNet (Neyshabur et al., 2020), and CIFAR-10-W (Sun et al., 2024)) for a class incremental learning (CIL) setup, we divide it into multiple disjoint tasks. We assume a disjoint setup (Parisi et al., 2019), where tasks do not share classes. We summarize the in-distribution (ID) domain, the out-of-distribution (OOD) domains, the total number of classes per dataset, the number of classes per task, and the number of tasks for each dataset in Tab. 6. Within each dataset, all tasks have the same size, except PACS, which has a total of 7 classes. For PACS, the first task includes 3 classes, while the subsequent tasks include data for 2 classes each. For CIFAR-10-W, even though CIFAR-10 Krizhevsky et al. (2009) can use MA data, the image resolution of CIFAR-10 is 32×32 , while CIFAR-10-W has a resolution of 224×224 , leading to performance degradation. Therefore, we exclude comparison with MA in the CIFAR-10-W experiments. For multi-modal visual-concept incremental learning (MVCIL) setup, we summarize the the total number of concepts, number of tasks, and number of concepts per task in Tab. 7.

Note that we run five different task splits using five different random seeds and report the average and standard error of the mean (SEM) for all experiments.

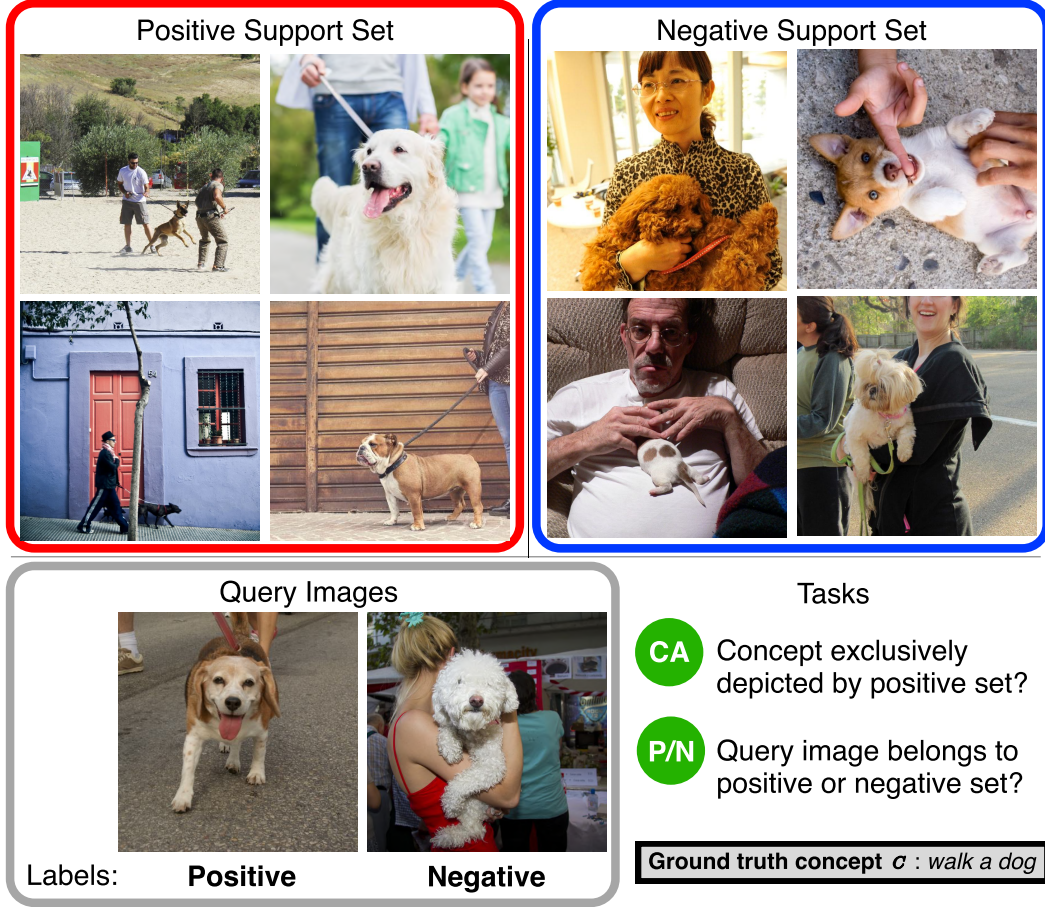


Figure 4: **An example of the Bongard-HOI task.** CA refers to the concept answering task, while P/N refers to the classifying whether a query image belongs to the positive or negative set.

Dataset	ID domain	OOD domains	total # of classes	# of tasks	# of classes / task
PACS	Photo	Art, Cartoon, Sketch	7	3	2 (only initial task: 3)
DomainNet	Real	Clipart, Painting, Sketch	345	5	69
CIFAR-10-W	-	CIFAR-10-W	10	5	2

Table 6: **Task configurations for the CIL setup on each domain generalization dataset.**

Dataset	Form of Concepts	total # of concepts	# of tasks	# of concepts / task
Bongard-OpenWorld	Free-form	10	5	2
Bongard-HOI	(action, object)	50	5	10

Table 7: **Task configurations for the MVCIL setup on each Bongard benchmark.**

A.3 IMPLEMENTATION DETAILS

We used ResNet18 (He et al., 2016) and Vision Transformer (ViT) (Dosovitskiy & Brox, 2016) as network architectures for the class-incremental learning (CIL) setup. Due to the large number of parameters in ViT, training it from scratch in an online setup resulted in lower performance. Therefore, we used the weights of a model pre-trained on ImageNet-1K (Russakovsky et al., 2015) as initial weights for ViT. For data augmentation, we consistently applied RandAugment (Cubuk et al., 2020) in all experiments. For the optimizer and the learning rate (LR) scheduler in CIL setup, we employed the Adam optimizer with initial LR of 0.0003 and Constant LR scheduler, respectively, following prior works (Koh et al., 2023; Seo et al., 2024b). In MVCIL setup, we use Adam optimizer with LR 5×10^{-5} and Constant LR scheduler. For task split, we adopt a disjoint setup, where tasks

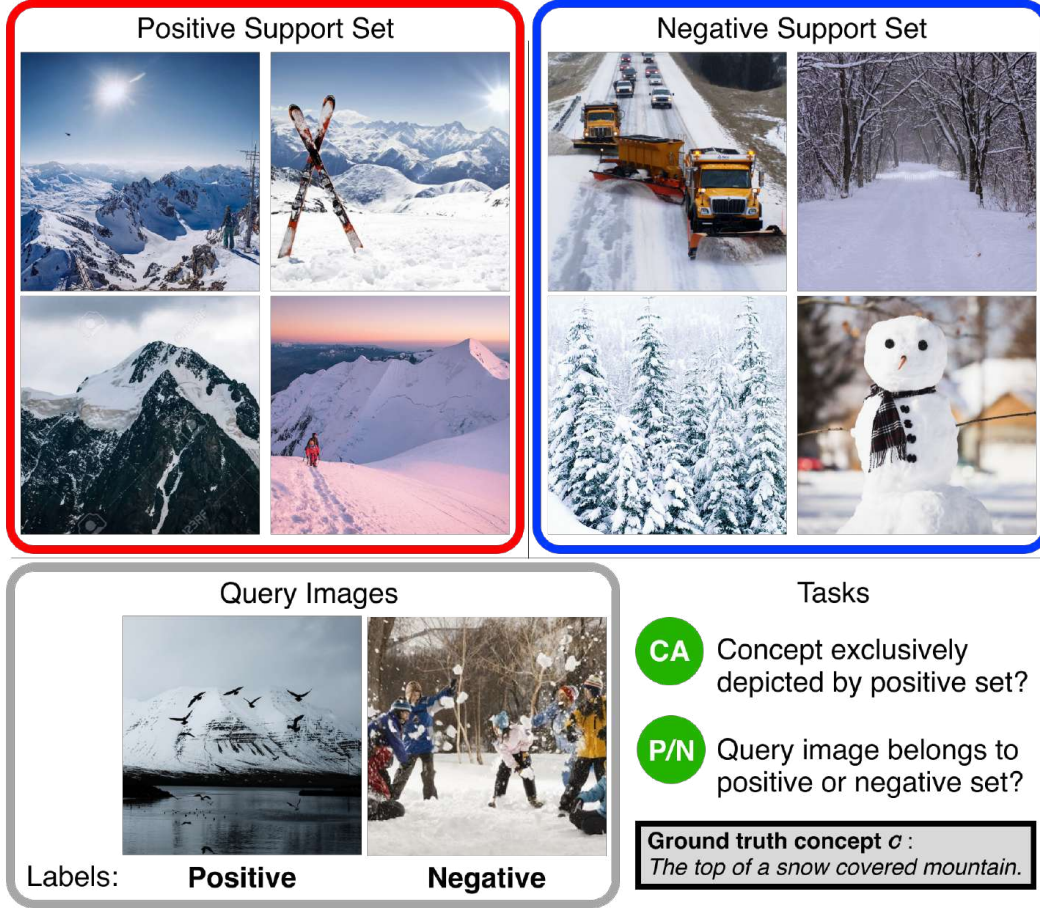


Figure 5: **An example of the Bongard-OpenWorld task.** CA refers to the concept answering task, while P/N refers to the classifying whether a query image belongs to the positive or negative set. The concept c is free-form, such as sentences.

do not share classes (Parisi et al., 2019). We used the GPT-4 model (Achiam et al., 2023) for all LLM-based prompt generation baselines including HIRPG. To ensure a fair comparison among manually annotated data, generated data, and web-scraped data, we used an equal number of samples in all experiments. Regarding the web-scraped data, we obtained 20% more samples than necessary for batch training with the aim of filtering out noisy data. To achieve this, we utilized pre-trained CLIP (Radford et al., 2021) for filtering, which excludes the most noisy bottom samples, resulting in a cleaned subset used for training, following (Schuhmann et al., 2022). We used $8 \times$ RTX 4090 GPUs to generate images using text-to-image generative models.

Hyperparameters. For T , which refers to the temperature of the softmax function in CONAN, is uniformly set to 0.5 across all datasets. For L , the truncation ratio used in RMD score normalization, we set it to 5% for all experiments. In all experiments, we run five different random seeds and report the average and standard error mean. For diverse prompt generation, we generate 50 different prompts for all baselines across all benchmarks, including HIRPG, to ensure a fair comparison. Specifically, to generate 50 prompts using HIRPG, we set depth $d = 2$, and $K = 7$ for all setups.

Following (Koh et al., 2021; 2023; Kim et al., 2024a), we conduct batch training for each incoming sample. Specifically, for PACS, CIFAR-10, and DomainNet, the number of batch iterations per incoming sample is set to 2, 2, and 3, respectively, with batch sizes of 16, 16, and 128. Episodic memory sizes are configured as 200, 2000, and 10000 for PACS, CIFAR-10-W, and DomainNet, respectively.

For MVCIL setups, the number of batch iterations per incoming sample is set to 0.5, with a batch size of 2, and a memory size of 500 in both Bongard-HOI and Bongard-OpenWorld. Unlike the CIL

setup, where data is composed solely of image and label pairs, in the MVCIL setup, each set contains both negative and positive examples corresponding to a given concept. We store 500 sets in episodic memory. In MVCIL benchmarks, *i.e.*, Bongard-HOI and Bongard-OpenWorld, we used 2 positive images and 2 negative images for a support set and 4 positive images and 4 negative images for a support set, respectively. For the MVCIL setup, we use the LLaVA-1.5-7B (Liu et al., 2023b).

Prompts. For the prompt diversification module ψ , we use the following system prompt to sequentially generate the prompts:

To generate images using a text-to-image generation model, I need to create a prompt. Keep the domain photorealistic and use different visual scenes and visual styles or different color profiles/palettes. Here is a list of prompts that I have previously generated <previous outputs>. Please create a new prompt that does not overlap with these.

In Bongard-HOI-P/N, we use the following prompt:

'positive' images:<|endofchunk|><image><image>
 'negative' images:<|endofchunk|><image><image>
 'query' image:<|endofchunk|><image>
 Given 2 'positive' images and 2 'negative' images, where both 'positive' and 'negative' images share a 'common' object, and only 'positive' images share a 'common' action whereas 'negative' images have different actions compared to the 'positive' images, the 'common' action is exclusively depicted by the 'positive' images. And then given 1 'query' image, please determine whether it belongs to 'positive' or 'negative' You must choose your answer from the Choice List. Choice list:[Positive, Negative].
 Your answer is:

In Bongard-HOI-CA, we use the following prompt:

'positive' images:<|endofchunk|><image><image>
 'negative' images:<|endofchunk|><image><image>
 Given 2 'positive' images and 2 'negative' images, where both 'positive' and 'negative' images share a 'common' object, and only 'positive' images share a 'common' action whereas 'negative' images have different actions compared to the 'positive' images, the 'common' action is exclusively depicted by the 'positive' images. Your job is to find the 'common' action within the 'positive' images. You must choose your answer from the Choice List. Choice List: [choice lists].
 Your answer is:

In Bongard-OpenWorld-P/N, we use the following prompt:

'positive' images:<|endofchunk|><image><image><image><image>
 'negative' images:<|endofchunk|><image><image><image><image>
 Given 4 'positive' images and 4 'negative' images, where 'positive' images share 'common' visual concepts and 'negative' images cannot, the 'common' visual concepts exclusively depicted by the 'positive' images. Here, 'common' sentence from 'positive' images is common concept. And then given 1 'query' image, please determine whether it belongs to 'positive' or 'negative'.

In Bongard-OpenWorld-CA, we use the following prompt:

'positive' images:<|endofchunk|><image><image><image><image>
 'negative' images:<|endofchunk|><image><image><image><image>
 Given 4 'positive' images and 4 'negative' images, where 'positive' images can be summarized as 1 'common' sentence and 'negative' images cannot, the 'common' sentence describes a set of concepts that are common to 'positive' images. Please give the 'common' sentence from 'positive' images.

A.4 SELECTING HARD NEGATIVE CONCEPTS IN GENCL ON MVCIL SETUPS

For Bongard-HOI benchmark, Given a (object, concept), *e.g.*, (ride, a bike), GenCL retrieves hard negative concept using an LLM and the following prompt:

To train a model that distinguishes between positive and negative images, you need to choose N negative actions from the following negative action list. When choosing negative actions, you should consider the available actions from the object. For example, if the object is 'bird', possible actions are 'chase', 'feed', 'no interaction', 'watch', etc. If the object is 'orange', possible actions are 'cut', 'hold', 'no interaction', 'peel', etc. You should choose hard negative actions that are clearly distinguishable from positive actions among the possible actions.
 object: <object class>
 positive action: <positive action>
 negative action list: <action set>
 Please select a total of N negative actions. The response format must be strictly result: ['negative action1', 'negative action2', ...], and all negative actions must be included in the negative action list.

For Bongard-OpenWorld benchmark, GenCL retrieves hard negative concept using an LLM and the following prompt:

To create an image using a text-to-image generation model, I want to create a prompt. Below, a prompt for a positive image will be provided, and the goal is to generate a prompt for a negative image. It is important that the negative prompt partially overlaps with the positive prompt and has slight differences. For example, if the positive prompt is 'Dogs are running', then 'Dogs are drinking water' would be the negative prompt. Please create N 'negative' prompt sentences (under 5 words) that fits this description. Please ensure the response format is strictly 'prompt: answer'.
 Positive prompt: <positive prompt>.

A.5 COMPARISON OF HIRPG WITH DIVERSE PROMPT GENERATION METHODS.

To evaluate the effectiveness of HIRPG in diverse prompt generation, we further analyze the generated images based on two attributes: Recognizability (Fan et al., 2024), which evaluates whether the images accurately represent the intended concepts, and Diversity (Naeem et al., 2020), which assesses the variation among the images. Although we aim to generate diverse images using varied prompts, the generated images should accurately represent the desired concepts. For a fair comparison, we generate 50 text prompts using each prompt diversification baseline and use SDXL to generate the same number of images for all baselines, including HIRPG. We summarize the results in Tab. 8.

Method	PACS		DomainNet	
	Recognizability \uparrow	Diversity \uparrow	Recognizability \uparrow	Diversity \uparrow
LE (He et al., 2023b)	65.39	0.27	38.49	0.31
CHB (Sarıyıldız et al., 2023)	62.96	0.16	41.57	0.24
SC (Tian et al., 2024a)	71.50	0.19	33.19	0.20
CCG (Hammoud et al., 2024)	68.78	0.18	32.71	0.19
HIRPG (Ours)	90.77	0.31	52.83	0.35

Table 8: **Comparison of prompt diversification methods.** We compare the Recognizability and Diversity of images generated using text prompts derived from prompt generation methods in conjunction with a text-to-image generative model.

The model trained with data generated by HIRPG significantly outperforms those trained with data generated by the baselines in both the in-distribution (ID) and out-of-distribution (OOD) domains. Furthermore, as shown in the Recognizability and Diversity, HIRPG not only generates more diverse data, but also produces more recognizable data compared to baselines. Overall, DomainNet exhibits higher Diversity. This is because, despite having approximately 50 times more classes than PACS, it has fewer images per class, resulting in a smaller number of generated images per prompt. For detailed descriptions of the baselines and metrics (*i.e.*, Rec and Div), see Sec. A.10 and Sec. A.16, respectively.

A.6 QUALITATIVE ANALYSIS

We qualitatively compare web-scraped images, manually annotated images, and GenCL-generated images, highlighting diversity and recognizability of GenCL-generated images.

Multi-modal Visual-concept Incremental Learning Setup. We compare samples acquired through different data acquisition methods for the given concept in the Bongard-HOI and Bongard-OpenWorld datasets, as shown in Fig.6 and Fig.7, respectively. In Fig. 6, although the desired positive images are related to ‘ride a bike’, the web-scraped positive set includes images of ‘not ride a bike’, such as ‘sitting on a bike’. In addition, the positive set for ‘riding a bike’ contains even an image of a road with a bicycle symbol painted on it. These inherent noises in web-scraped data, *i.e.*, the inclusion of unwanted or irrelevant content, can significantly hinder model performance, as discussed in Sec. 1. In contrast, GenCL leverages the controllability (Nie et al., 2021) of the generative model, *i.e.*, the ability to generate the desired output through text descriptions, allowing it to produce the intended images.

Similarly, in Fig. 7, GenCL effectively generates both positive and negative support sets. In contrast, web-scraped data include images that do not match the given concept ‘A leopard relaxing on a tree branch.’ This discrepancy arises from the lengthy and free-form concepts used in Bongard OpenWorld, such as descriptive sentences, compared to the simpler object-action combinations in Bongard-HOI. In web scraping, those detailed and lengthy search queries may yield unrelated results.

Note that GenCL relies solely on positive concepts, as mentioned in Sec. 5.2. Specifically, in manually annotated (MA) data, high-quality annotators not only select positive support sets but also curate hard negative examples for the negative sets. In contrast, GenCL utilizes only positive concepts (*i.e.*, concepts that the model needs to learn) and automatically generates hard negative examples using text prompts created by large language models (LLMs), as demonstrated in Sec. A.4. Nonetheless, as shown in Fig. 6 and Fig. 7, the negative samples generated by GenCL are not clearly distinct from the positive examples, which enhances the model’s ability to differentiate between the concepts.

Class Incremental Learning Setup. We compare samples acquired through different baselines in the CIL setup, as illustrated in Fig. 8 and Fig. 9.



Figure 6: **Samples using different data acquisition methods for the same concept in the MVCIL setup.** The given concept is ‘ride a bike’ from the Bongard-HOI benchmark. The left four images represent positive examples that depict the given concept, while the right four images represent negative examples that illustrate different concepts. Here, ‘MA’ refers to manually annotated data.

A.7 EXPANDING GENCL TO THE JOINT TRAINING SETUP

We extend our proposed GenCL to the standard learning setup (*i.e.*, joint training setup), where all concepts to be learned are provided at once. In this setting, we compare GenCL not only with training-based methods, such as GLIDE, but also with training-free methods (*i.e.*, CLIP-ZS (Radford et al., 2021), SuS-X-SD (Udandarao et al., 2023), VisDesc (Menon & Vondrick, 2023), SD-Clf (Li et al., 2023), and CUPL (Pratt et al., 2023)) that leverage pre-trained Vision-Language Models (VLMs), such as CLIP (Radford et al., 2021) or generative models, such as SDXL (Podell et al., 2023). Note that although these methods do not update model weights, they generate images for support sets or create customized prompts using LLMs to classify the target concept. We provide a detailed explanation of training-free baselines in Sec. A.12.

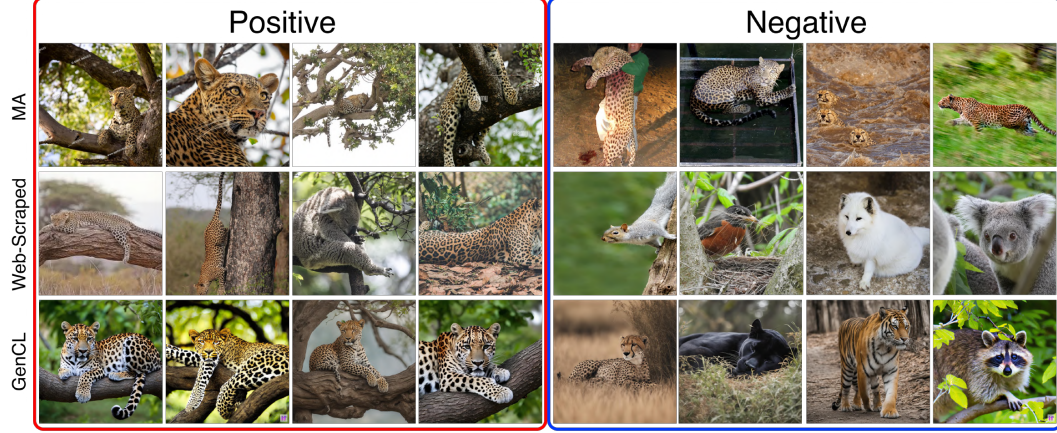


Figure 7: **Samples using different data acquisition methods for the same concept in the MVCIL setup.** The given concept is ‘*A leopard relaxing on a tree branch*’ from the Bongard-OpenWorld benchmark. The left four images represent positive examples that depict the given concept, while the right four images represent negative examples that illustrate different concepts. Here, ‘MA’ refers to manually annotated data.

We first compare these methods using the same model, *i.e.*, ResNet-50-CLIP, a CLIP model with ResNet-50 as the vision encoder. For this, we utilize the YFCC100M (Thomee et al., 2016) pre-trained CLIP model. We summarize the results in Tab. 9. For training-dependent methods, we train the model for 10 epochs, ensuring the same amount of data is used across all baselines for a fair comparison. As shown in the table, GenCL significantly outperforms existing name-only classification baselines, as well as combinations of baselines with our proposed data ensemble method, *i.e.*, CONAN. Furthermore, compared to diverse prompt generation baselines (LE, CHB, SC, and CCG), our proposed HIRPG outperforms in both setups—with and without CONAN—demonstrating the effectiveness of our proposed components in a joint training setup.

Next, we compare the results with those obtained using only the CLIP-pretrained ResNet-50 for training-dependent methods. While the same model (*i.e.*, CLIP) can be employed for training-free methods, training vision-language models (VLMs) demands substantial computational resources, which impedes real-time adaptation and limits their deployment in real-world applications (Koh et al., 2021; Caccia et al., 2022). Therefore, to improve training efficiency and enable faster adaptation to newly encountered concepts, we also compare the results of training solely on the vision encoder of the CLIP model for training-dependent methods. To assess training efficiency, we train them for 10 epochs, consistent with Tab. 9, and summarize the results in Tab. 10.

As shown in the table, several training-free methods outperform GenCL in the in-domain (ID) scenario. This advantage arises because they utilize off-the-shelf CLIP models, which are pre-trained on large-scale datasets, particularly in the photo domain, which we consider as ID in our experiments. However, despite the benefits of large-scale pre-training, these methods struggle to generalize in out-of-domain (OOD) scenarios, such as the sketch and painting domains.

In contrast, GenCL not only outperforms all baselines but also surpasses a model trained with manually annotated data in the OOD domains of both PACS and DomainNet. This demonstrates that large-scale pre-training alone does not guarantee good generalization across all downstream tasks, highlighting the necessity of few-epoch training for personalization and real-time adaptation in name-only setup.

A.8 ABLATION STUDY OF GENCL USING THE ViT

In addition to Sec. 5.3, we conduct an ablation study on two components of GenCL, namely HIRPG and CONAN, using the ImageNet-pretrained ViT-base model. We use the same number of images for each baseline to ensure a fair comparison, and summarize the results in Tab. 5.

Similar to the ablation study with ResNet-18, both components significantly enhance performance in both in-distribution (ID) and out-of-distribution (OOD) domains.

A.9 ABLATION STUDY OF HIRPG

We conduct an ablation study on HIRPG to investigate the benefits of each proposed component, namely hierarchical generation (HIG) and recurrent prompt generation (RPG), in PACS and DomainNet. For a fair comparison, we generate 50 different prompts and use SDXL to generate images for all baselines. For HIG,

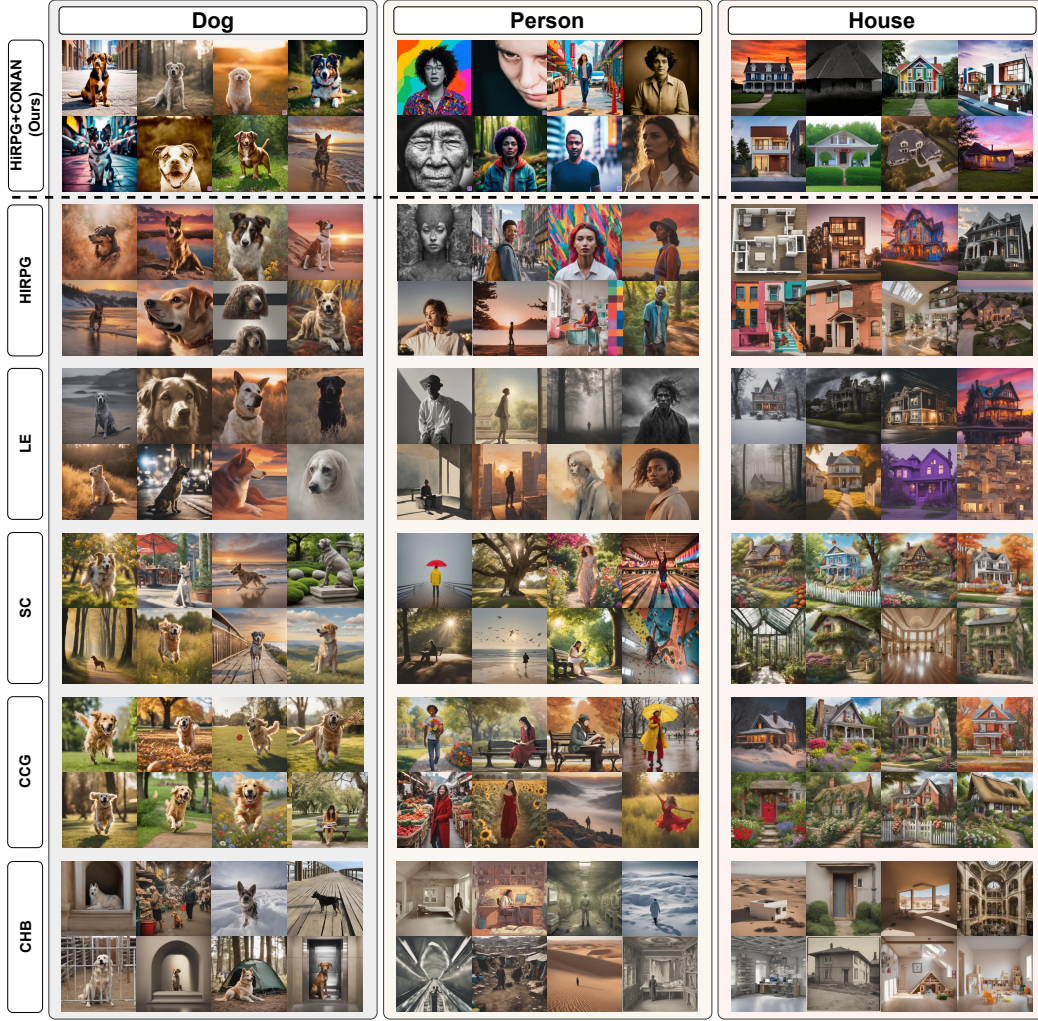


Figure 8: **Samples using different data acquisition methods for the same concept in the CIL setup.** The given concepts are *Dog*, *Person*, *House*, which are from PACS.

we use a 7-ary tree with a depth of 2. Since we only need 50 prompts, we sample 50 prompts from the 57 total nodes of a complete 7-ary tree.

The results are summarized in Tab. 11. In the table, vanilla prompt generation refers to generating N different prompts using an LLM without applying RPG or HIG. Specifically, we use the following prompts for vanilla prompt generation:

To generate images using a text-to-image generation model, I need to create 50 prompts. Keep the domain photorealistic and use different visual scenes and visual styles or different color profiles/palettes. Please create 50 prompts that does not overlap with each other. Please ensure that each response includes the word '[concept]'. For example, 'A photo of a [concept].', 'A detailed sketch of [concept].', 'A hyper-realistic portrait of [concept].', etc.

As shown in the table, applying RPG alone even degrades the performance compared to vanilla prompt generation. This degradation occurs because, as iterative steps progress, the length of the LLM input increases, making it challenging to utilize the information within the extended context effectively (*i.e.*, *lost-in-the-middle challenge* (Liu et al., 2024; An et al., 2024)), as discussed in Sec. 4.1. In contrast, combining RPG with HIG addresses the lengthy input problem, leading to improved performance in both in-distribution (ID) and out-of-distribution on PACS and DomainNet.

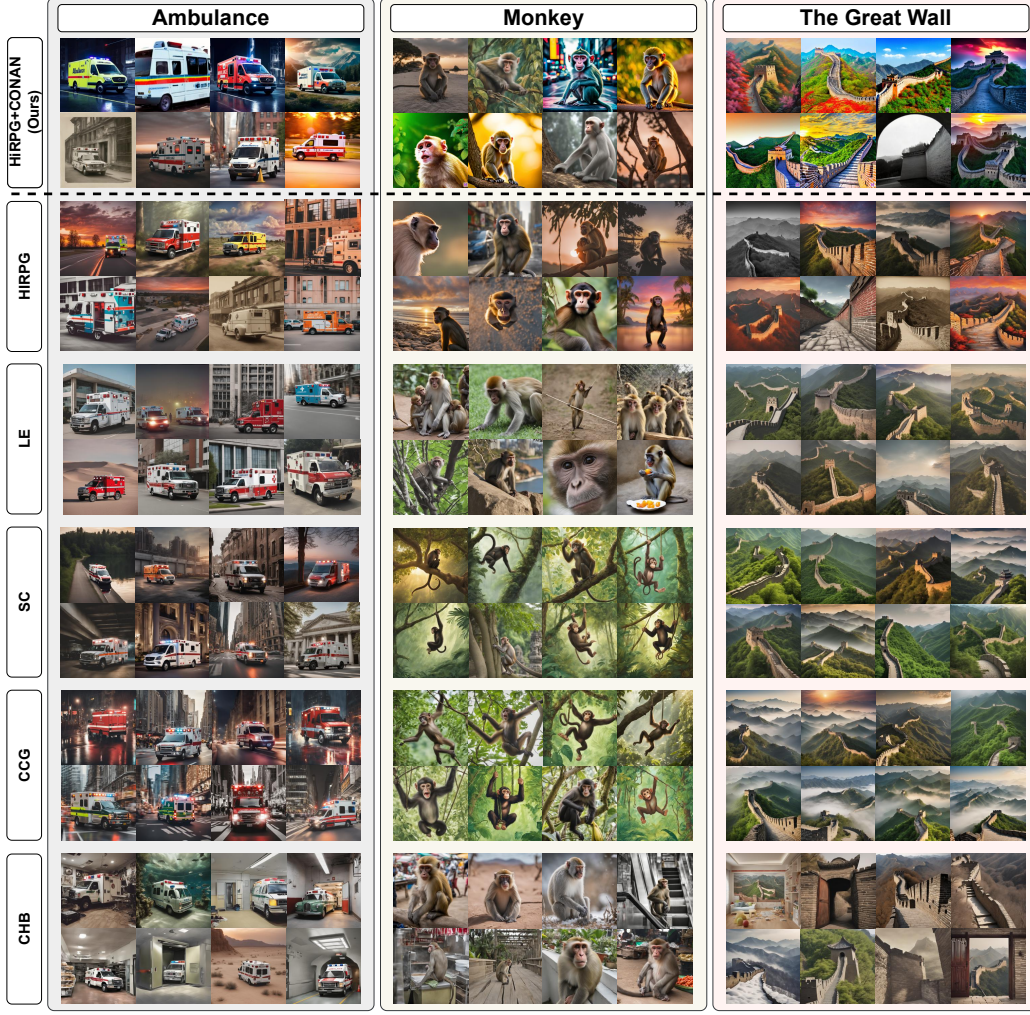


Figure 9: Samples using different data acquisition methods for the same concept in the CIL setup. The given concepts are *Ambulance*, *Monkey*, *The Great Wall*, which are from DomainNet.

A.10 PROMPT DIVERSIFICATION AND CONCEPT-SPECIFIC PROMPT GENERATION BASELINES

For a fair comparison, we used the same number of diversified prompts (*i.e.*, 50) for all prompt diversification methods, including our proposed HCFG. Moreover, for all LLM-based prompt generators, we consistently used GPT-4o (Wu et al., 2024c) as LLM.

LE (He et al., 2023b). LE leverages an off-the-shelf word-to-sentence T5 model, pre-trained on the “Colossal Clean Crawled Corpus” dataset (Raffel et al., 2020) and fine-tuned on the CommonGen dataset (Lin et al., 2020), to increase the diversity of language prompts and generated images, with the aim of better harnessing the potential of synthesized data. Specifically, the category names are entered into the word-to-sentence model, which generates diversified sentences containing the category names. These diversified sentences are then used as prompts for the text-to-image generation process.

CCG (Hammoud et al., 2024). For a given concept set C , CCG (Concept-based Captions Generation) uses an LLM generator G_{LLM} to produce concept-specific prompts for T2I models. The designed prompt p for each concept $c \in C$ is structured as follows:

Type	Training Data	CIFAR-10-W	DomainNet	
		OOD	ID	OOD
Training-free	CLIP-ZS (Radford et al., 2021)	57.14	14.69	5.17
	SuS-X-SD (Udandarao et al., 2023)	53.08	20.06	7.5
	VisDesc (Menon & Vondrick, 2023)	51.83	16.87	6.52
	CuPL (Pratt et al., 2023)	50.5	18.25	6.36
	CALIP (Guo et al., 2023)	51.62	16.43	6.39
	SD-Clf (Li et al., 2023)	52.48	12.27	11.85
Training-dependent	Glide-syn (He et al., 2023b)	55.93	38.26	9.31
	LE (He et al., 2023b)	73.51	47.43	14.7
	(+) CONAN	75.13	52.87	17.26
	CHB (Sarıyıldız et al., 2023)	70.61	45.28	14.62
	(+) CONAN	75.96	52.31	17.49
	SC (Tian et al., 2024a)	71.3	40.42	12.36
	(+) CONAN	75.04	49.64	15.19
	CCG (Hammoud et al., 2024)	58.25	39.32	11.57
	(+) CONAN	63.14	42.94	14.37
	HIRPG	74.47	52.30	20.18
	(+) CONAN (Ours)	77.64	54.85	22.66
	Manually Annotated	59.12	71.13	20.29

Table 9: **Quantitative comparison between different name-only baselines on joint training setup.** We employ the YFCC100M pre-trained ResNet50-CLIP, which uses ResNet50 as the vision encoder for the CLIP model, for all methods.

Type	Training Data	PACS		DomainNet	
		ID	OOD	ID	OOD
Training-free	CLIP-ZS (Radford et al., 2021)	99.11	49.12	14.69	5.17
	SuS-X-SD (Udandarao et al., 2023)	95.55	47.81	20.06	7.5
	VisDesc (Menon & Vondrick, 2023)	93.77	46.09	16.87	6.52
	CuPL (Pratt et al., 2023)	89.32	46.51	18.25	6.36
	CALIP (Guo et al., 2023)	92.58	48.43	16.43	6.39
	SD-Clf (Li et al., 2023)	92.58	48.43	12.27	11.85
Training-dependent	Glide-syn (He et al., 2023b)	85.16	33.2	29.02	6.73
	LE (He et al., 2023b)	88.43	38.03	40.74	10.47
	(+) CONAN	93.47	44.54	54.60	15.62
	CHB (Sarıyıldız et al., 2023)	83.38	30.98	35.97	9.60
	(+) CONAN	92.88	41.42	49.17	15.51
	SC (Tian et al., 2024a)	76.26	28.19	30.42	8.23
	(+) CONAN	85.46	42.05	44.66	12.01
	CCG (Hammoud et al., 2024)	81.01	31.71	26.59	6.89
	(+) CONAN	85.76	41.55	32.31	8.72
	HIRPG	89.91	43.98	46.19	17.80
	(+) CONAN (Ours)	94.36	60.75	51.85	21.01
	Manually Annotated	97.03	33.80	72.54	19.09

Table 10: **Quantitative comparison between different name-only baselines on joint training setup.** We employ the YFCC100M pre-trained ResNet50-CLIP for training-free methods, while for training-dependent methods, we utilize only the vision encoder of the CLIP model.

Method	PACS				DomainNet			
	ID		OOD		ID		OOD	
	$A_{AUC} \uparrow$	$A_{last} \uparrow$	$A_{AUC} \uparrow$	$A_{last} \uparrow$	$A_{AUC} \uparrow$	$A_{last} \uparrow$	$A_{AUC} \uparrow$	$A_{last} \uparrow$
Vanila Prompt Generation	47.74±1.52	47.30±2.38	31.66±1.45	25.41±0.66	20.82±0.39	17.19±0.34	7.09±0.21	5.55±0.11
(+) RPG	45.55±1.55	47.60±1.90	32.07±1.70	25.53±1.74	17.62±0.35	13.96±0.25	6.88±0.15	5.30±0.11
(+) HIG + RPG (Ours)	51.36±2.59	51.63±2.49	34.12±1.27	28.18±1.32	27.72±0.30	23.71±0.39	10.70±0.19	8.75±0.13

Table 11: **Benifits of components of the proposed prompt generation method.** RPG refers to the recurrent prompt generation and HIG refers to the hierarchical generation. Vanilla prompt generation refers to generating 50 different prompts using an LLM without incorporating RPG or HIG.

Your task is to write me an image caption that includes and visually describes a scene around a concept. Your concept is c . Output one single grammatically correct caption that is no longer than 15 words. Do not output any notes, word counts, facts, etc. Output one single sentence only.

Formally, the set of generated captions for concept c can be defined as $T = \{t_{c,n} \sim G_{LLM}(p, c)\}, \forall c \in C, \forall n \in \{1, 2, \dots, N\}$, where N is the number of desired prompts for each concept.

CHB (Sarıyıldız et al., 2023). To increase the visual diversity of the output images, CHB (Concept Name + Hypernym + Background) combines background information along with hypernyms, which helps reduce semantic ambiguity. They assume that class c can be seen ‘inside’ a scene or background. Therefore, to enhance visual diversity, CHB combines the concept name and its hypernym (as defined by the WordNet (Miller, 1995) graph) with scene classes from the Places365 dataset (López-Cifuentes et al., 2020) as background for each concept. Formally, p_c can be defined as " $p_c = c, h_c \text{ inside } b$ ", where c refers to the concept name, h_c refers to the hypernym of the concept c , and b refers to the background.

SC (Tian et al., 2024a). SC (Synthesizing captions) consider three types of templates for each concept c : $c \rightarrow \text{caption}$, $(c, bg) \rightarrow \text{caption}$, and $(c, rel) \rightarrow \text{caption}$.

- $c \rightarrow \text{caption}$. They generate a sentence directly from the concept name c using LLM.
- $(c, bg) \rightarrow \text{caption}$. Similar to CHB (Sarıyıldız et al., 2023), they combine the visual concept c with a background bg . However, while CHB randomly selects bg from the Places365 dataset, they generate a list of suitable backgrounds for the chosen concepts using LLM, which helps avoid unlikely combinations, such as a blue whale on a football field.
- $(c, rel) \rightarrow \text{caption}$. They consider pairing a given visual concept c with a positional relationship word rel , such as "in front of." To add variety, rel is randomly selected from a predefined set of 10 relationship words. Using an LLM, they then generate captions that reflect the selected relationship word in relation to the concept.

A.11 DATA ENSEMBLE BASELINES

Gradient-based methods (Killamsetty et al., 2021b;a; Shin et al., 2023) minimize the distance between the gradients from the entire dataset T and from the selected coreset S ($S \subset T$) as follows:

$$\min_{\mathbf{w}, S} \left\| \sum_{(x,y) \in T} \frac{\nabla_{\theta} l(x, y; \theta)}{|T|} - \sum_{(x,y) \in S} \frac{w_x \nabla_{\theta} l(x, y; \theta)}{\|\mathbf{w}\|_1} \right\|_2, \quad (5)$$

where \mathbf{w} is the vector of learnable weights for the data in selected coreset S , l refers to the loss function, θ denotes the model parameters, and $\|\cdot\|_1, \|\cdot\|_2$ represent the L1 norm and L2 norm, respectively. To solve Eq. 5, **GradMatch** (Killamsetty et al., 2021a) uses orthogonal matching pursuit algorithm (Elenberg et al., 2016), while **CRAIG** (Mirzasoleiman et al., 2020) uses submodular maximization.

LCMat (Shin et al., 2023). While Craig and GradMatch minimize the gradient difference between T and the S , LCMat matches the loss curvatures of the T and S over the model parameter space, inspired by the observation that a loss function L quantifies the fitness of the model parameters θ under a specific dataset. Specifically, they claim that even though optimizing S toward T with respect to θ would decrease the loss difference between T and S in θ (i.e., $|L(T; \theta) - L(S; \theta)|$), if the loss difference increases with a small perturbation ϵ in θ (i.e., $|L(T; \theta + \epsilon) - L(S; \theta + \epsilon)|$), it indicates a lack of generalization on $\theta + \epsilon$, or an over-fitted reduction of S by θ . Since this generalization failure on the locality of θ subsequently results in the

large difference of loss surfaces between T and S , they propose an objective that maximize the robustness of θ under perturbation ϵ as follows:

$$\min_S (L_{abs}(T, S; \theta + \epsilon) - L_{abs}(T, S; \theta)), \quad (6)$$

where L_{abs} refers to the loss difference between T and S on θ (i.e., $L(T; \theta) - L(S; \theta)$).

Moderate (Xia et al., 2023). Moderate selects data points with scores close to the score median, using the median as a proxy for the score distribution in statistics.

Specifically, given a well-trained feature extractor $f(\cdot)$ and the full training data $T = \{t_1, t_2, \dots, t_n\}$, the process begins by computing the hidden representations (or embeddings) of all data points in T , i.e., $\{z_1 = f(t_1), z_2 = f(t_2), \dots, z_n = f(t_n)\}$. Next, the ℓ_2 distance from the hidden representation of each data point to the class prototype of its corresponding class is calculated. Formally, for a sample t belonging to class c , its distance $d(t)$ is given by $d(t) = \|z - z^c\|_2$, where $z = f(t)$ and z^c is the prototype of class c . Subsequently, all data points are sorted in ascending order according to their distance, which are denoted by $\{d(\tilde{t}_1), d(\tilde{t}_2), \dots, d(\tilde{t}_n)\}$. Finally, data points near the distance median are selected as the coreset S .

Uncertainty (Coleman et al., 2020). Uncertainty suggests that data samples with a lower level of confidence in model predictions will have a greater influence on the formation of the decision boundary. For uncertainty scores, we utilize Entropy, following the approach of Shin et al. (2023), among the methods LeastConfidence, Entropy, and Margin.

Glister (Killamsetty et al., 2021b). Glister is a generalization-based data selection method that optimizes generalization error via a bi-level optimization problem to select the coreset S , aiming to maximize the log-likelihood on a held-out validation set.

A.12 DESCRIPTION OF NAME-ONLY CLASSIFICATION BASELINES.

Glide-Syn (He et al., 2023b). This approach takes *category name* as input and employs the word-to-sentence T5 model (pre-trained on ‘Colossal Clean Crawled Corpus’ dataset (Raffel et al., 2020) and finetuned on ‘CommonGen’ dataset (Lin et al., 2019)), to generate diverse concept-specific sentences. After generating diverse sentences using the word-to-sentence T5 model, they generate corresponding images using prompts and the Glide (Nichol et al., 2021) text-to-image generative model. Finally, they introduce a clip filter to reduce noise and enhance robustness.

CLIP-ZS (Radford et al., 2021). CLIP-ZS refers to zero-shot classification using a pre-trained CLIP model, where the model classifies images without any additional training, leveraging its knowledge from large-scale pre-training. Since CLIP is pre-trained on large-scale web dataset, it demonstrates impressive zero-shot performance (Qian et al., 2024).

SuS-X-SD (Udandara et al., 2023). This approach uses generated SuS (Support Sets) to ensure accurate predictions for target categories by taking only categories as input. Specifically, SuS-X-SD generates support sets using Stable Diffusion (Podell et al., 2023) and uses them as a combination with the pre-trained vision language model and an adapter module named TiP-X for inference.

CuPL (Pratt et al., 2023). While the standard zero-shot open vocabulary image classification model, e.g., CLIP (Radford et al., 2021), uses only the set of base prompts, i.e., ‘A photo of {category name}’, and target images for classification, CuPL proposes to use customized prompts using LLM. Specifically, they propose using GPT-3 (Brown et al., 2020), but we replace it with GPT-4o (Wu et al., 2024c), which is a stronger LLM and the one used in our proposed GenCL, for a fair comparison.

CALIP (Guo et al., 2023). CALIP enhances the zero-shot performance of CLIP (Radford et al., 2021) by introducing a parameter-free attention module. This module enables visual and textual representations to interact and explore cross-modal informative features via attention. As a result, image representations are enriched with textual-aware signals, and text representations are guided by visual features, leading to better adaptive zero-shot alignment.

SD-Clf (Li et al., 2023). SD-Clf leverages large-scale text-to-image diffusion models, such as Stable Diffusion (Podell et al., 2023), for classification tasks. Given an input x and a finite set of classes C , the model computes the class-conditional likelihoods $p_\theta(x|c)$. By selecting an appropriate prior distribution $p(c)$ and applying Bayes’ theorem, SD-Clf predicts class probabilities $p(c|x)$, effectively classifying the input based on the computed likelihoods.

A.13 JUSTIFICATION FOR THE USE OF RMD SCORE

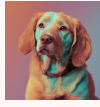

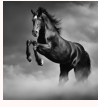





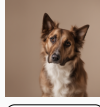
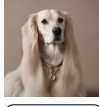






	Dog		Horse		Guitar		Elephant	
High RMD, High RS								
	RMD: 4.4 RS: 49.17	RMD: 4.7 RS: 41.48	RMD: 4.9 RS: 41.14	RMD: 5.2 RS: 40.39	RMD: 4.3 RS: 41.55	RMD: 4.6 RS: 37.09	RMD: 4.4 RS: 37.71	RMD: 4.9 RS: 41.99
Low RMD, Low RS								
	RMD: 0.3 RS: 28.54	RMD: 1.5 RS: 30.91	RMD: 1.4 RS: 29.82	RMD: 1.7 RS: 31.72	RMD: 0.6 RS: 26.9	RMD: 0.5 RS: 24.67	RMD: 0.4 RS: 29.16	RMD: 2.1 RS: 26.12

Figure 10: Examples of samples with high RMD & high Rarity scores, as well as samples with low RMD & low Rarity scores. The average RMD scores for Dog, Horse, Guitar, and Elephant are 2.91, 3.03, 2.43, and 3.25, respectively, while the corresponding average Rarity scores are 33.59, 33.58, 33.57, and 33.18.

Many recent works endeavor to assess the diversity (Naeem et al., 2020; Han et al., 2022; Kim et al., 2024b), complexity (Hwang et al., 2023), aesthetics (Somepalli et al., 2024; Khajehabdollahi et al., 2019), and realism (Chen et al., 2023a; 2024; 2023b) of the generated images. In our work, we use the relative Mahalanobis distance (RMD) score (Cui et al., 2023), to evaluate the complexity of the generated samples. The reason for selecting RMD is its independence from the need for real samples in its calculation, while other diversity metric, such as the Rarity Score (Han et al., 2022) and the TopP&R (Kim et al., 2024b) requires *real* samples, *i.e.*, data that have not been generated. Note that our proposed framework, GenCL, operates exclusively with *concept* inputs rather than *real* data, thus we cannot access *real* data.

As we can see in Fig. 10, the Rarity score and the RMD score exhibit similar trends, showing the ability of the RMD score to effectively measure complexity even in the absence of real samples.

A.14 COMPARISON BETWEEN CONAN AND VARIOUS RMD-BASED ENSEMBLE

We compare CONAN with various RMD-based ensemble approaches in PACS, and summarize the result in Tab. 12. The table reveals that CONAN significantly outperforms others in both In-Distribution (ID) and Out-of-Distribution (OOD) evaluations. Furthermore, with the exception of **CONAN**, all ensemble methods even exhibit a decrease in performance compared to the scenario where no ensembling¹ is applied. The k -highest RMD ensemble, which excludes easy samples, leads to insufficient learning in the class-representative region, while the k -lowest RMD concentrates solely on easy samples, resulting in limited diversity. Inverse CONAN employs the inverse of the probabilities utilized in CONAN. Similar to the k -lowest RMD ensemble, it tends to prioritize easy samples, resulting in limited diversity and accuracy loss.

Ensemble Method Δ	ID		OOD	
	$A_{AUC} \uparrow$	$A_{last} \uparrow$	$A_{AUC} \uparrow$	$A_{last} \uparrow$
No ensembling	51.36 \pm 2.59	51.63 \pm 2.49	34.12 \pm 1.27	27.18 \pm 1.32
Equal weight ensemble	50.56 \pm 2.32	50.03 \pm 2.13	35.49 \pm 1.41	27.13 \pm 3.44
k -highest RMD ensemble	52.80 \pm 2.82	50.09 \pm 3.06	36.24 \pm 1.52	30.09 \pm 1.35
k -lowest RMD ensemble	41.72 \pm 2.88	37.98 \pm 2.19	31.17 \pm 2.34	24.58 \pm 2.49
Inverse Prob	45.01 \pm 3.03	38.70 \pm 4.12	32.94 \pm 1.62	27.61 \pm 1.97
CONAN (Ours)	55.89\pm3.06	55.43\pm2.49	38.53\pm1.15	33.73\pm1.82

Table 12: Comparison of ensemble methods in PACS (Zhou et al., 2020), using ER (Rolnick et al., 2019) for all ensemble methods. The proposed ensemble method outperforms other ensemble methods. We used Photo domain as the ID domain, whereas we used Art, Cartoon, and Sketch domain as OOD domains. For OOD domains, A_{AUC} and A_{last} refer to the average value across all OOD domains.

¹No ensembling denotes the usage of images generated exclusively through SDXL (Podell et al., 2023).

A.15 DETAILS ABOUT DETERMINING ID AND OOD DOMAINS

To compare with the model trained with GenCL and the model trained with manually annotated (MA) data, we select one domain as MA data from each domain generalization benchmark.

A.16 DETAILS ABOUT METRICS

Area Under the Curve of Accuracy (A_{AUC}). In online CL setup, the model is trained using the stream data in real time, thus the model is used for inference at every moment rather than the predefined time point (*e.g.*, end of the task) (Koh et al., 2021; Caccia et al., 2022; Banerjee et al., 2023; Pellegrini et al., 2020). Therefore, to measure inference performance at any time, we evaluated the model at regular intervals during a specified evaluation period and then calculated the area under the accuracy curve, denoted A_{AUC} (Koh et al., 2021; Caccia et al., 2022; Koh et al., 2023), which is defined as follows:

$$A_{AUC} = \sum_{i=1}^k f(i\Delta n)\Delta n, \quad (7)$$

where the step size Δn is the number of samples encountered between inference queries and $f(\cdot)$ is the accuracy in the curve of the # of samples-to-accuracy plot. High A_{AUC} indicates that the model maintains good inference performance throughout the entire training process.

Recognizability. Following Boutin et al. (2022); Fan et al. (2024), we evaluate whether the images accurately represent the intended concepts by computing the F1 score for each class. As previous work utilized a pre-trained classifier (ViT-Base), we initialize the feature extractor with an ImageNet pre-trained ViT-Base. We then perform linear probing (Alain, 2016) on this model with a downstream dataset to train a classification head for the dataset. Recognizability is then calculated by averaging the F1 scores across all classes.

Diversity. To assess the diversity of generated images, Naeem et al. (2020) measures coverage, defined as the ratio of real samples encompassed by the generated samples. Specifically, they calculate the fraction of real samples whose k -nearest neighborhoods contain at least one generated sample. Formally, given the embedded real and generated data, represented by $\{X_i\}$ and $\{Y_j\}$ from an ImageNet pre-trained feature extractor, coverage is defined as:

$$\text{coverage} := \frac{1}{N} \sum_{i=1}^N 1_{\exists j \text{ s.t. } Y_j \in B(X_i, \text{NND}_k(X_i))}, \quad (8)$$

where $\text{NND}_k(X_i)$ denotes the distance from X_i to the k^{th} nearest neighboring among $\{X_i\}$ excluding itself and $B(x, r)$ denotes the sphere in \mathbb{R}^D around x with radius r .

Consensus-based Image Description Evaluation (CIDEr). CIDEr (Vedantam et al., 2015) aims to automatically evaluate how well a predicted sentence, s_p , matches the consensus of a set of ground-truth sentences, $S = \{s_{gt,1}, \dots, s_{gt,N}\}$. The intuition is that the measure of consensus should encode how often n -grams from the candidate sentence appear in the reference sentences. In contrast, n -grams that are absent from the reference sentences should not appear in the candidate sentence. To encode this intuition, they calculate the TF-IDF (Robertson, 2004) vectors for the n -gram elements within the candidate and reference sentences by computing the cosine similarity between the two vectors. Formally, CIDEr for n -grams is calculated as follows:

$$\text{CIDEr}_n(s_p, s_{gt}) = \frac{g^n(s_p) \cdot g^n(s_{gt})}{\|g^n(s_p)\| \|g^n(s_{gt})\|}, \quad (9)$$

where $g(s)$ represents the vectorized form of a sentence s , obtained by calculating the TF-IDF values for its n -gram elements. Finally, they combine the scores from n -grams of varying lengths as follows:

$$\text{CIDEr} = \frac{1}{N} \sum_{i=1}^N \text{CIDEr}_n. \quad (10)$$

Following Vedantam et al. (2015), we use $N = 4$ and define the set of ground truth sentences in the positive set as S .

A.17 DETAILS ABOUT GENERATORS \mathcal{G}

For the set of generators \mathcal{G} , we use five text-to-image generative models: SDXL (Podell et al., 2023), DeepFloyd IF², SD3 (Esser et al., 2024), CogView2 (Ding et al., 2022), and Auraflow³. As illustrated in Figure 11, different generators produce varied samples when prompted with identical prompts conditioned on the same concept.

²<https://github.com/deep-floyd/IF>

³<https://huggingface.co/fal/AuraFlow>

Details of each generator are as follows:

SDXL. SDXL is an enhanced latent diffusion model for text-to-image synthesis, building upon the previous versions of Stable Diffusion. Specifically, SDXL introduces three key improvements: (1) a UNet (Ronneberger et al., 2015) backbone that is 3× larger than in previous Stable Diffusion models, (2) an additional conditioning technique, and (3) a diffusion-based refinement model to further improve the visual quality of generated images.

DeepFloyd IF. DeepFloyd IF utilizes a frozen text encoder alongside three cascaded pixel diffusion stages. Initially, the base model produces a 64x64 image from a text prompt, which is then progressively enhanced by two super-resolution models to reach 256x256 and ultimately 1024x1024 pixels. At every stage, the model uses a frozen T5 transformer-based text encoder to derive text embeddings, which are then passed into a UNet.

CogView2. CogView2 pretrain a 6B-parameter transformer using a straightforward and adaptable self-supervised task, resulting in a cross-modal general language model (CogLM). This model is then fine-tuned for efficient super-resolution tasks. The hierarchical generation process is composed of three steps: (1) A batch of low-resolution images (20×20 tokens) is first generated using the pretrained CogLM. Optionally, poor-quality samples can be filtered out based on the perplexity of CogLM image captioning, following the post-selection method introduced in CogView (Ding et al., 2021). (2) These generated images are then upscaled to 60×60 -token images via a direct super-resolution module fine-tuned from the pretrained CogLM. (3) Finally, these high-resolution images are refined through another iterative super-resolution module fine-tuned from CogLM.

SD3. SD3 enhances current noise sampling methods for training rectified flow models (Liu et al., 2023c) by steering them toward perceptually significant scales. In addition, SD3 introduces a new transformer-based architecture for text-to-image generation, employing distinct weights for the two modalities. This design facilitates a bidirectional flow of information between image and text tokens, leading to improved typography, text comprehension, and higher human preference ratings.

AuraFlow. AuraFlow, inspired by SD3, is currently the largest text-to-image generation model. It introduces several modifications to SD3, including the removal of most MMDiT blocks (Esser et al., 2024) and their replacement with larger DiT encoder blocks (Peebles & Xie, 2023).

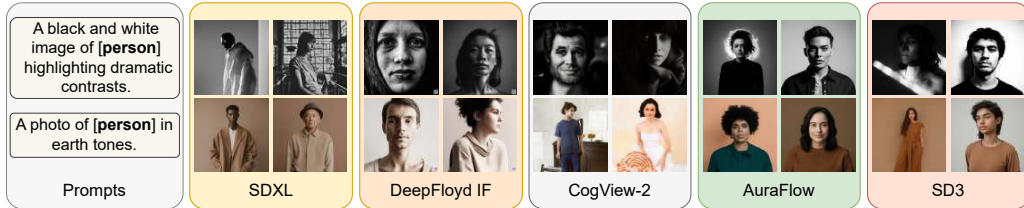


Figure 11: Examples of PACS (Zhou et al., 2020) generated samples from various generators using two of the prompt rewrites. Illustrations from the concept "Person" are showcased.

A.18 EXTENDED RELATED WORK

Methods for Continual Learning. Replay-based method, which stores data from previous tasks in episodic memory for replay, is one of the most widely used approaches, due to its effectiveness in preventing catastrophic forgetting (Zhang et al., 2023b; Yoo et al., 2024; Kozal et al., 2024). However, despite their effectiveness in preventing forgetting, they raise data privacy concerns due to the storage of real data from previous tasks in episodic memory. To address these privacy concerns, pseudo-replay approaches have been proposed (Graffieti et al., 2023; Thandiackal et al., 2021; Van de Ven et al., 2020; Shin et al., 2017; Van de Ven & Tolias, 2018), which leverage generative models to generate images of previous tasks instead of storing actual data in episodic memory. While these approaches utilize generative models similar to our GenCL framework, they still require manually annotated data to train the generative model (Shin et al., 2017; Van de Ven et al., 2020; Van de Ven & Tolias, 2018). In contrast, our GenCL framework eliminates the need for any manually annotated data, relying solely on the category names the model aims to learn.

A.19 MANUAL ANNOTATION VS. WEB-SCRAPING VS. GENERATIVE DATA

In modern deep learning, the trajectory of advancement is heavily influenced by the exponential growth of training data and the corresponding models trained on these vast datasets. Foundation models are typically exposed to datasets in the order of billions during training, obtained predominantly through web scraping (Schuhmann et al., 2022; Xue et al., 2020; Zhu et al., 2024; Gao et al., 2020; Kocetkov et al., 2022; Bain et al.,

2021). Although web scraping is a cost-effective method to produce high-quality datasets, studies underscore issues such as potential biases (Foerderer, 2023; Packer et al., 2018; Caliskan et al., 2017), copyright, privacy, and license concerns (Quang, 2021; Solon, 2019), and the risks of data contamination (Dekoninck et al., 2024; Li, 2023) or data leakage from evaluation (Balloccu et al., 2024).

As demonstrated in Fig. 1, we highlight the key differences between Manually Annotated (MA), Web scraped, and Generated data on six different axes: (a) Controllability, (b) Storage issues, (c) Usage restrictions, (d) Privacy issues, (e) Acquisition cost, and (f) Noise. In this section, we aim to provide the definition of each of these axes and their corresponding implications on each type of data source.

Controllability. encompasses the ability to generate or acquire images with various contexts, backgrounds, settings, and themes as desired. It pertains to the ability to obtain images depicting different concepts in compositions not commonly found in natural environments, as well as in domains relevant to the task at hand. Under this definition, we assert that the MA data exhibit low controllability. This limitation arises from its reliance on data captured from a finite set of scenarios or sensors, which inherently restricts the breadth of diverse settings where the concept can be observed. Web-scraped data also suffer from low controllability for the same reasons. In contrast, the generated data have high controllability due to the ability of foundation text-to-image (T2I) generators to produce diverse images for each concept through varied prompting.

Storage Issues. Storing extensive data, locally or in the cloud, imposes additional costs, which can become impractical in environments constrained by limited total storage capacity. In addition, transmitting large, substantial data samples in a federated setup can face challenges arising from bandwidth and latency bottlenecks. In such contexts, depending on a large corpus of MA data becomes counterintuitive. On the other hand, both web-scraped and generated data present themselves as cost-effective alternatives for accessing substantial data volumes without necessitating explicit storage expenditures.

Usage Restrictions. encompass limitations imposed on the use of images for training machine/deep learning models, typically due to copyright or licensing protections. These restrictions arise from various legal frameworks across different demographics, regulating, and sometimes prohibiting, the training of models on protected data for commercial deployment. This challenge is particularly prevalent in web-scraped data, where the abundance of protected data may not be adequately filtered (Khan & Hanna, 2020). In contrast, MA data bypass this issue, as it is presumed that the data are filtered or obtained from a proprietary source with appropriate permissions during annotation. Notably, generated data offer a more advantageous position, as they do not necessitate such filtering and encounter limited or no usage restrictions, thereby providing a readily available solution to issues arising from data protection concerns.

Privacy Issues. may arise when data samples inadvertently leak or explicitly contain sensitive, confidential, or private user information. Examples of such images could include those featuring people’s faces (O’Sullivan, 2020; Murgia & Harlow, 2019) or personal objects that disclose identity-related details, such as addresses or financial assets. Once again, web data emerge as the primary source vulnerable to issues stemming from the use of private data, an issue extensively present in web-scraped data (Subramani et al., 2023; Wenger et al., 2022; Solon, 2019; Lukas et al., 2023). MA data are expected to be protected from privacy concerns due to prior filtering or explicit agreement on data usage prior to annotation. In comparison, generated data should ideally not contain private data. Furthermore, several recent works (Chen et al., 2018; 2019; Carvalho et al., 2022; Xu et al., 2023) have explored methods to enforce fairness and differential privacy in data synthesis, offering solutions for identity protection.

Acquisition Cost. refers to the total expenses incurred in obtaining a specific number of data samples necessary to train or evaluate the learner f_θ for a particular task. As emphasized in 1, MA data entail a substantial acquisition cost, primarily due to the expenses associated with densely annotating the data through human workers. This, coupled with the rigorous filtering process, makes MA data prohibitively expensive to acquire at scale. Although web data do not require such significant financial outlay for annotation, they do require intensive filtering, which contributes to an elevated cost and poses a barrier to constructing large datasets solely from web sources. In contrast, due to the advantages in controllability, generated data boast a notably low acquisition cost for generating large and diverse datasets.

Noise. pertains to instances where data that are not related to a concept are erroneously labeled as belonging to that concept. It may also mean discrepancies between the context of the data and the associated concept. As highlighted in Sec. A.24, web data often exhibit a high degree of noise, necessitating extensive filtering or label correction processes. In contrast, both MA data and generated data are less susceptible to such noise. In the case of MA data, the presumption of prior filtering serves as a primary solution to mitigate noisy data. Meanwhile, for generated data, the advantages of controllability enable the mitigation of noise resulting from inconsistencies in concept-image alignment. Despite the drawback of requiring GPU usage, T2I model inference incurs lower costs compared to MA due to its ability to generate pure images, making it a more cost-effective option.

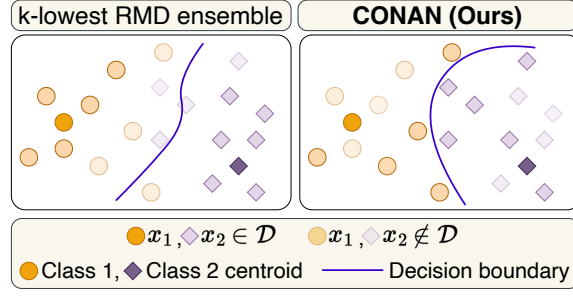


Figure 12: **CONAN** helps in finding a tighter decision boundary due to having a higher probability of including high RMD scored samples in the ensemble of generated data \mathcal{D} . Intuitively, high RMD scored samples are farther away from their class prototype but closer to other class samples in comparison to low RMD scored samples which are concentrated closer around the class prototype. Note that CONAN includes not only high RMD samples but also some low RMD (*i.e.*, class-representative) samples.

A.20 DETAILS OF RMD SCORE CALCULATION

The RMD (Cui et al., 2023) score of a sample (x_i, y_i) is defined as follows:

$$\begin{aligned}\mathcal{RMD}(x_i, y_i) &= \mathcal{M}_{cls}(x_i, y_i) - \mathcal{M}_{agn}(x_i), \\ \mathcal{M}_{cls}(x_i, y_i) &= -(G(x_i) - \mu_{y_i})^T \Sigma^{-1} (G(x_i) - \mu_{y_i}), \\ \mathcal{M}_{agn}(x_i) &= -(G(x_i) - \mu_{agn})^T \Sigma_{agn}^{-1} (G(x_i) - \mu_{agn}),\end{aligned}\tag{11}$$

where G represents the feature extractor, $\mathcal{M}_{cls}(x_i, y_i)$ denotes the Mahalanobis distance from $G(x_i)$ to the corresponding class mean vector $\mu_{y_i} = \frac{1}{N_i} \sum_{y_j=y_i} G(x_j)$, with N_i being the count of samples labeled as y_i , Σ^{-1} denotes the inverse of the averaged covariance matrix across classes. Furthermore, $\mathcal{M}_{agn}(x_i)$ represents the class-agnostic Mahalanobis distance, where μ_{agn} denotes the overall sample mean, and Σ_{agn}^{-1} denotes the inverse covariance for the class-agnostic case.

In the online CL setup, where data arrive in a continuous stream, it is not feasible to calculate μ and Σ of the entire dataset. Instead, a necessity arises to continuously update these statistical parameters to accommodate the dynamic nature of the incoming data stream.

Starting with the initially computed mean vector μ_{y_i} and the covariance matrix Σ from N samples, the arrival of a new sample x_{N+1} triggers an update. The updated mean vector μ_{new} is computed incrementally using a simple moving average (SMA), as follows:

$$\mu_{new} = \frac{N\mu_{old} + x_{N+1}}{N+1}.\tag{12}$$

Similarly, we calculate Σ using a simple moving variance. Specifically, the update for the new covariance matrix Σ_{new} is calculated using the deviation of the new sample from the old mean $\Delta = x_{N+1} - \mu_{old}$, and its deviation from the new mean $\Delta_{new} = x_{N+1} - \mu_{new}$.

Formally, we formulate the update process as follows:

$$\Sigma_{new} = \frac{1}{N+1} \left(N\Sigma_{old} + \Delta\Delta_{new}^T \right).\tag{13}$$

The update process for the class-agnostic mean vector μ_{agn} and covariance Σ_{agn} follows the same incremental approach as described for the class-specific components.

CONAN includes a significant number of samples with high RMD scores in the ensemble dataset. Not only does it include samples with the highest RMD scores, but it also probabilistically incorporates samples with low RMD scores. This approach ensures a core-set ensemble, and we illustrate the effect of CONAN in Fig. 12

A.21 SCALING BEHAVIOR

Recent scaling law studies (Hernandez et al., 2021; Hoffmann et al., 2022) offer predictive insight into model performance by scaling computation, data, and model capacity. Despite the limited exploration of scaling in continual learning settings (Ramasesh et al., 2022), and particularly with synthetic data (Fan et al., 2024) being confined to static frameworks, our empirical analysis in Fig. 13 delves into scaling dynamics with varying proportions of generated data for online continual learning setup.

For ResNet18 (He et al., 2016) and ViT (Dosovitskiy & Brox, 2016), we observe a consistent linear improvement trend in both ID and OOD A_{AUC} as the volume of generated data increases, across the PACS (Zhou et al., 2020) dataset. This scaling behavior underscores the positive correlation between performance improvement and larger generated data ensembles in online continual learning, reinforcing the rationale for the use of generators in the absence of annotated data.

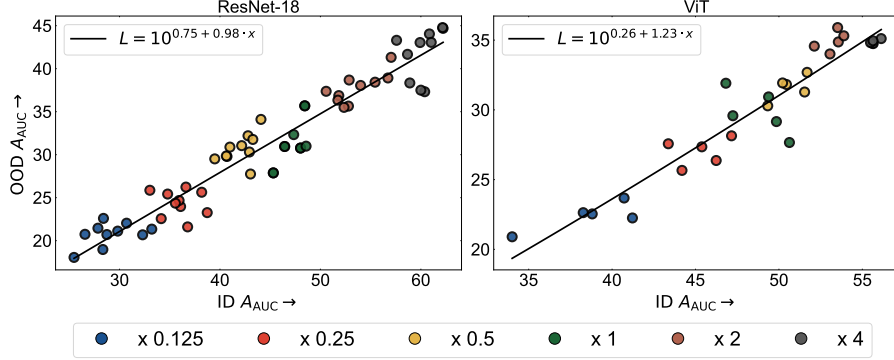


Figure 13: Ensemble scaling behavior of (a) ResNet18 (He et al., 2016) and (b) ViT (Dosovitskiy & Brox, 2016) for ID A_{AUC} vs. OOD A_{AUC} on the PACS dataset (Zhou et al., 2020) using ER (Rolnick et al., 2019). ($\times 1$) denotes the ensemble volume in primary experiments, the default data budget.

A.22 EXPERIMENTAL RESULTS ON CIFAR-10-W

We compared manually annotated (MA) data and generated data using CONAN on CIFAR-10-W (Sun et al., 2024). As mentioned in Sec. 5.1, since CIFAR-10-W only contains data on the OOD domains of CIFAR-10, we evaluated only the performance of the out-of-distribution (OOD) domain.

Additionally, since CIFAR-10-W is a web-scraped dataset, the domain of CIFAR-10-W and the web-scraped data are the same. Therefore, we excluded web-scraped data in experiments on CIFAR-10-W and only evaluated OOD performance. We summarize the results in Tab. 13.

Method	CIFAR-10-W	
	$A_{AUC} \uparrow$	$A_{last} \uparrow$
Glide-Syn (ICLR 2023)	47.14 \pm 0.80	34.13 \pm 0.54
LE (ICLR 2023)	47.20 \pm 0.67	34.03 \pm 0.60
(+) CONAN	51.69 \pm 0.70	41.32 \pm 1.38
CHB (CVPR 2023)	45.30 \pm 0.62	31.20 \pm 0.54
(+) CONAN	51.29 \pm 0.72	37.06 \pm 1.77
SC (CVPR 2024)	44.75 \pm 0.62	30.41 \pm 0.84
(+) CONAN	48.60 \pm 0.63	36.39 \pm 0.88
CCG (arXiv 2024)	38.96 \pm 0.94	24.71 \pm 0.70
(+) CONAN	41.32 \pm 0.99	28.94 \pm 0.77
HIRPG	52.52 \pm 0.37	41.04 \pm 1.26
(+) CONAN (Ours)	55.53\pm0.41	43.51\pm1.13

Table 13: Quantitative comparison between different diverse prompt generation baselines on CIFAR-10-W.

A.23 PSEUDOCODE FOR THE GENCL

Algorithm 1 provides a detailed pseudocode for GenCL. When a new concept is encountered, the prompt generation module ψ generates concept-specific prompts. These prompts are then used by a set of T2I generators G to create concept-specific images. Subsequently, the ensembler Δ selects a coresct from these generated images for efficiency, instead of training on the entire dataset. The continual learner is then trained using this selected ensemble set. During training, GenCL also stores a small portion of previously generated samples in episodic memory M . Although GenCL can generate images related to previously encountered concepts, retaining these samples helps to reduce computational overhead.

Algorithm 1 GenCL

```

1: Input Model  $f_\theta$ , Prompt generation module  $\psi$ , Set of Generators  $\mathcal{G}$ , Ensembler  $\Delta$ , Concept
   stream  $\mathcal{C}$ , Learning rate  $\mu$ , Episodic memory  $\mathcal{M}$ 
2: for  $y \in \mathcal{Y}$  do ▷ New concept arrives from concept stream  $\mathcal{Y}$ 
3:   Generate  $\mathcal{P}_c \leftarrow \psi(c)$  ▷ Generate prompt set  $\mathcal{P}_c$  for a given concept  $c$  using  $\psi$ 
4:   Generate  $\{\mathcal{X}_c^{(i)}\}_{i=1}^{|G|} \leftarrow \mathcal{G}(\mathcal{P}_c)$  ▷ Generate image set  $\mathcal{X}_c$  using  $\mathcal{G}$  and  $\mathcal{P}_c$ 
5:    $(\mathcal{X}_c, c) \leftarrow \Delta(\{\mathcal{X}_c^{(i)}\}_{i=1}^{|G|})$  ▷ Ensemble generated image set using ensembler  $\Delta$ 
6:    $\mathcal{L} = \mathcal{L}_{CE}(f_\theta(\mathcal{X}_c), c)$  ▷ Calculate cross entropy loss
7:   Update  $\theta \leftarrow \theta - \mu \cdot \nabla_\theta \mathcal{L}$  ▷ Update model
8:   Update  $\mathcal{M} \leftarrow \text{ReservoirSampler}(\mathcal{M}, (X_c, c))$  ▷ Update episodic memory
9: end for
10: Output  $f_\theta$ 

```

Algorithm 2 RPG

```

1: Input Maximum number of leaf nodes of  $K$ -ary Tree  $K$ , System prompt  $P_s$ , Large language
   model  $LLM$ , Prompt of parent node  $P_{d,k}$ 
2:  $\mathcal{P} \leftarrow \emptyset$  ▷ Initialize the generated prompt set  $\mathcal{P}$ 
3:  $k' \leftarrow 1$  ▷ Initialize the number of child node of  $P_{d,k}$ 
4: while  $k' \leq K$  do ▷ Generate  $k'_{th}$  child node of  $P_{d,k}$ 
5:   if  $k' = 1$  then
6:      $P_{d+1,k'} \leftarrow LLM(P_s, P_{d,k})$ 
7:   else
8:      $P_{d+1,k'} \leftarrow LLM(P_s, P_{d,k} \cup \mathcal{P})$  ▷ Recurrently forward the previously generated prompts  $\mathcal{P}$ 
9:   end if
10:   $\mathcal{P} \leftarrow \mathcal{P} \cup \{P_{d+1,k'}\}$  ▷ Add the currently generated prompts to  $\mathcal{P}$ 
11:   $k' \leftarrow k' + 1$ 
12: end while
13: Output  $\mathcal{P}$ 

```

Algorithm 3 HIRPG

```

1: Input Newly encountered concept  $y$ , Maximum number of leaf nodes of  $K$ -ary Tree  $K$ , Prompt
   of parent node  $P_{d,k}$ 
2:  $\mathcal{P} \leftarrow \text{RPG}(P_{d,k})$  ▷ Generate  $K$  number of prompts using RPG
3:  $\mathcal{P}_{ch} \leftarrow \emptyset$  ▷ Initialize the prompt set generated from the child nodes
4: if  $d < D$  then
5:   for  $P_{k'} \in \mathcal{P}$  do
6:      $\mathcal{P}_{ch} \leftarrow \mathcal{P}_{ch} \cup \text{HIRPG}(P_{k'}, d + 1)$  ▷ Merge prompt generated in child nodes
7:   end for
8: end if
9: Output  $\mathcal{P} \cup \mathcal{P}_{ch}$  ▷ Merge the prompts generated in the child nodes and the current node, then return

```

Additionally, Algorithm 3, Algorithm 4, Algorithm 5 provide a detailed pseudo code for prompt generation module ψ , a set of generators \mathcal{G} , ensembler Δ , respectively, which are components of GenCL.

A.24 DETAILS ABOUT WEB-SCRAPPING

For web-scrapping, we follow C2C (Prabhu et al., 2024), which proposes scraping data from the web using category names. C2C (Prabhu et al., 2024) uses four search engines, including Flickr, Google, Bing, and DuckDuckGo, using the publicly available querying tool⁴ to collect URLs. While C2C uses four search engines for scraping, we only use three search engines, *i.e.*, Flickr, Google, and Bing, since ICrawler did not support web data scraping from DuckDuckGo at the time of our attempt on February 20, 2024. After collecting the URLs from each search engine, we use a multi-threaded downloader⁵ to quickly download the images, following (Prabhu et al., 2024). For Flickr, we are able to download approximately 500 images per minute due to the rapid URL

⁴<https://github.com/hellock/icrawler>

⁵<https://github.com/rom1504/img2dataset>

Algorithm 4 Set of Generators \mathcal{G}

```

1: Input Rewritten prompt set  $\mathbf{P}$ , Generative models  $\mathcal{G} = \{g_1, g_2, \dots, g_{|\mathcal{G}|}\}$ 
2:  $U_1, \dots, U_{|\mathcal{G}|} \leftarrow \emptyset, \dots, \emptyset$  ▷ Initialize the sets of generated images for each model
3: for  $p \in \mathbf{P}$  do
4:   for  $g_i \in \mathcal{G}$  do
5:     Generate  $x_y^{(i)} \leftarrow g_i(p)$  ▷ Generate image  $x_y^{(i)}$  using prompt  $p$  and generative model  $g_i$ 
6:      $U_i \leftarrow U_i \cup \{x_y^{(i)}\}$  ▷ Append  $x_y^{(i)}$  to the set  $U_i$ 
7:   end for
8: end for
9: Output  $\{U_1, U_2, \dots, U_{|\mathcal{G}|}\}$  ▷ Return the generated image sets for each model

```

Algorithm 5 Ensembler Δ

```

1: Input Generated image sets  $\{U_1, U_2, \dots, U_{|\mathcal{G}|}\}$ , Coreset size  $|V|$ , Temperature parameter  $\tau$ 
2:  $U \leftarrow \bigcup_{i=1}^{|\mathcal{G}|} U_i$  ▷ Combine all generated image sets into a single set  $U$ 
3: for each sample  $(x_i, y_i) \in U$  do
4:   Compute  $\mathcal{RMD}(x_i, y_i) \leftarrow \mathcal{M}(x_i, y_i) - \mathcal{M}_{\text{agn}}(x_i)$  ▷ Compute RMD scores for each sample
5: end for
6: Truncate  $\mathcal{RMD}(x_i, y_i)$  ▷ Remove outliers from RMD scores
7: Normalize  $\mathcal{RMD}(x_i, y_i) \leftarrow \mathcal{RMD}(x_i, y_i)$  ▷ Apply Z-score normalization
8: Compute selection probability  $p_{x|y} = \frac{e^{\mathcal{RMD}_{x|y}/\tau}}{\sum_{x' \in U} e^{\mathcal{RMD}_{x'|y}/\tau}}$  for each  $x \in U$  ▷ Compute the selection probability using softmax function
9: Select  $V \leftarrow \text{Sample } |V| \text{ images from } U \text{ based on probabilities } p_{x|y}$ 
10: Output Coreset  $V$ 

```

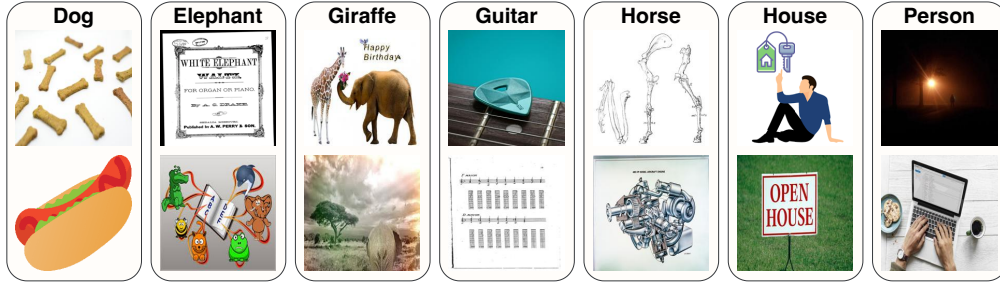


Figure 14: Examples of noisy raw data obtained via web-scraping for the classes in the PACS dataset.

collection facilitated by the official API. Meanwhile, for Google and Bing, the download rate is slower, at approximately 100 images per minute on a single CPU machine. However, the download rate depends on the network conditions and the status of the API and the search engine. In C2C, the ensemble of web-scraped data from search engines is weighted differently for each benchmark. For example, in the Stanford Cars benchmark, the weights are Google: Bing: Flickr = 5:4:2, while in the Flowers benchmark, they are 1:1:2, respectively. Since we use different benchmarks compared to C2C, we select equal weight selection to ensemble web-scraped data, *i.e.*, Google: Bing: Flickr = 1:1:1, which is one of the most straightforward and widely used ensemble techniques (Shahhosseini et al., 2022; Ju et al., 2018).

Datasets scraped from search engines such as Flickr, Google, and Bing contain uncurated (*i.e.*, noisy) samples. To clean these datasets, following (Schuhmann et al., 2022), we use a pre-trained CLIP (Radford et al., 2021) model to measure the similarity between the images and corresponding prompts. Specifically, we scraped 10% more data than the required dataset size (*i.e.*, the number of manually annotated data) and removed samples with a low CLIP similarity score for each experiment. Although prior work (Prabhu et al., 2024) addressed the ambiguity of queries through manual query design, such as adding an auxiliary suffix to refine queries, in an online CL scenario, where new concepts stream in real-time, such hand-crafted query designs for each concept are limited.

In summary, data noise, network dependency, and the need for manual query design specific to each concept restrict the use of web-scraped data in real-world scenarios where new concepts are encountered in real-time.

A.25 QUALITATIVE RESULTS FOR PROMPT GENERATION METHODS

We also qualitatively evaluate the performance of our proposed prompt generation method, HIRPG, against existing prompt diversification baselines, including LE, CHB, SC, and CCG. The comparison is illustrated across multiple concepts from the PACS and DomainNet datasets, as shown in Table 14, Table 15, Table 16, and Table 17. We observe that most methods are not able to generate diverse prompts as well as maintain coherence and logic across generated instances. Common issues across baseline methods include irrelevant content, repetitions, and overused phrases.

LE generates repetitive phrases across difference concepts that, while slightly different in wording, essentially convey the same meaning. In Table 14 and Table 15, despite that phrases differ in their choice of words, they describe the same visual concept: a subject illuminated by soft, warm light, typically seen at sunrise or sunset. CHB, on the other hand, generate prompts with nonsensical combinations of objects and environments, such as "horse inside a bakery" or "house inside an aquarium". While diverse, the prompts are not grounded in reality, which limits their practical use in downstream tasks.

SC and CCG methods produce more coherent and consistent prompts. However, they show a tendency toward redundancy, particularly in descriptors like "majestic" and "gallops" for the *horse* concept, or "charming" and "rustic" for the *house* concept, reducing the overall uniqueness of the generated prompts. Compared to these existing prompt diversification baselines, our proposed prompt generation method, HIRPG, successfully captures not only the diversity but also the originality and coherence within its generated prompts.

A.26 EXTENDED QUANTITATIVE ANALYSIS

We perform additional comparisons with various combinations of diverse prompt generation baselines and data ensemble methods on DomainNet, and summarize the results in Tab. 18. For all data ensemble methods, including our proposed CONAN, we select an equal number of samples for the coreset to ensure a fair comparison. As shown in the table, CONAN is not only effective when combined with HIRPG, but also shows strong performance when paired with other prompt generation baselines, demonstrating its plug-and-play applicability across various methods.

A.27 LIMITATIONS AND FUTURE WORK

While CONAN provides a foundational strategy for optimal generator ensembling, we acknowledge limitations arising from the use of curated prompt rewrites without incorporating feedback from the continual learner. In addition, we acknowledge limitations associated with the fact that the generative model cannot produce high-quality images in all domains without fine-tuning.

In future endeavors, our aim is to expand the GenCL framework into multi-concept settings, leveraging and enhancing the compositional generation capabilities of T2I models. This extension encompasses broadening the proposed framework to dense prediction tasks such as semantic segmentation and object detection, and tasks in other modalities such as code generation.

Concept	Method	Examples
Horse	LE	<ul style="list-style-type: none"> • A calm horse illuminated by the first light of morning. • A sunrise horse bathed in warm orange hues. • A dew-drenched horse in vibrant sunset colors. • A serene horse under a pastel sunrise. • A peaceful horse bathed in the soft glow of dawn.
	CHB	<ul style="list-style-type: none"> • horse equine inside aquarium • horse equine inside bakery • horse equine inside music studio • horse, equine inside wave • horse, equine inside pizzeria
	SC	<ul style="list-style-type: none"> • A majestic horse stands gracefully in the middle of a sun-dappled apple orchard, surrounded by rows of apple-laden trees and the sweet fragrance of ripe fruit filling the air. • A majestic horse stands in a lush green pasture, its mane flowing gracefully in the gentle breeze • A majestic brown horse with a glossy coat stands gracefully in a sunlit meadow, surrounded by lush green grass and blooming wildflowers. • A majestic horse stands gracefully in a sunlit meadow, its coat shimmering in the golden rays of the setting sun. • A majestic horse stands gracefully in a lush, green meadow, its mane gently blowing in the breeze.
	CCG	<ul style="list-style-type: none"> • A majestic brown horse gallops freely through a sunlit meadow of wildflowers. • A majestic horse gallops through a sunlit meadow with wildflowers swaying in the breeze. • A majestic brown horse gallops freely across a sunlit, grassy meadow surrounded by blooming wildflowers. • A majestic horse gallops across a sunlit field, mane flowing in the breeze. • A majestic horse gallops through a sunlit meadow, its mane flowing in the breeze.
	HIRPG	<ul style="list-style-type: none"> • A high-contrast black and white photograph of horse. • A serene watercolor painting of horse. • A vibrant photo of horse during sunrise with a warm color palette. • A vivid painting of horse using vibrant colors. • A cinematic wide-angle shot of horse at dusk.

Table 14: Prompt samples using different prompt generation methods for the concept *Horse* from PACS dataset. Irrelevant content, repetitions, and overused phrases are marked in red, brown, and turquoise respectively.

Concept	Method	Examples
House	LE	<ul style="list-style-type: none"> • A calm house illuminated by the first light of morning. • A sunrise house bathed in warm orange hues. • A dew-drenched house in vibrant sunset colors. • A serene house under a pastel sunrise. • A peaceful house bathed in the soft glow of dawn.
	CHB	<ul style="list-style-type: none"> • house, building inside aquarium • house, building inside bakery • house, building inside music studio • house, building inside wave • house, building inside pizzeria
	SC	<ul style="list-style-type: none"> • house => A charming, rustic house with ivy-covered walls and a thatched roof, nestled amidst a flourishing garden of vibrant, blooming flowers, creating a serene and picturesque scene. • A charming countryside house with a thatched roof and ivy-covered walls, surrounded by a lush, colorful garden blooming with flowers on a sunny day • A charming rustic house stands besides a tranquil pond, surrounded by lush greenery and vibrant blooming plants, reflecting its serene image in the still water. • A charming rustic house, nestled in a vibrant, colorful garden filled with blooming flowers and tall trees, creating a picturesque and cozy scene. • A charming rustic house stands besides a tranquil pond, surrounded by lush greenery and vibrant blooming plants, reflecting its serene image in the still water.
	CCG	<ul style="list-style-type: none"> • A cozy, red-brick house with a white picket fence stands amidst colorful autumn trees. • A cozy, rustic house stands peacefully surrounded by vibrant autumn trees and a cobblestone path.. • A cozy, rustic house nestled in a forest, surrounded by vibrant autumn leaves and tall trees. • A cozy countryside house stands surrounded by vibrant autumn foliage under a clear, blue sky. • A cozy wooden house surrounded by colorful autumn trees under a clear blue sky.
	HIRPG	<ul style="list-style-type: none"> • A high-contrast black and white photograph of house. • A serene watercolor painting of house. • A vibrant photo of house during sunrise with a warm color palette. • A vivid painting of house using vibrant colors. • A cinematic wide-angle shot of house at dusk.

Table 15: Prompt samples using different prompt generation methods for the concept *House* from PACS dataset. Irrelevant content, repetitions, and overused phrases are marked in red, brown, and turquoise respectively.

Concept	Method	Examples
Diving Board	LE	<ul style="list-style-type: none"> • Scuba diver lands on the dry seas with his bare feet on a • The man with the green board doing darts is really nice. • Man in the snow at the beach... the guy on the scuba boat... • Man on the seaboard while diving • A man is caught in a sea of dolphins scuba diving on a
	CHB	<ul style="list-style-type: none"> • diving board, springboard inside home office • diving board, springboard inside bakery • diving board, springboard inside music studio • diving board, springboard inside subway station • diving board, springboard inside pizzeria
	SC	<ul style="list-style-type: none"> • A sleek, modern diving board extends over a pristine pool at an indoor diving facility, brightly lit with natural light streaming through large windows, casting reflections on the water's surface below. • A sleek diving board extends over a shimmering blue swimming pool, surrounded by lush greenery and bustling with activity under the bright summer sun. • A sleek diving board extends over an oceanview pool, with the shimmering blue waters of the ocean and a clear sky stretching out in the background. • On a serene summer day, a sleek diving board extends over a sparkling zero-entry pool, inviting swimmers to take the plunge into its crystal-clear, gradually deepening waters. • A sleek diving board extends over a crystal-clear synchronized swimming pool, surrounded by vibrant, choreographed swimmers creating mesmerizing patterns in the water.
	CCG	<ul style="list-style-type: none"> • A young girl prepares to leap off a wooden diving board into a sparkling pool below. • A young girl jumps joyously off a colorful diving board into the sparkling blue pool below. • A young girl poised on the diving board, ready to leap into the sparkling pool below. • A young girl leaps joyfully off a high diving board into a sparkling blue pool. • A young girl stands poised on a diving board, ready to leap into the sparkling pool.
	HIRPG	<ul style="list-style-type: none"> • A high-contrast black and white photograph of diving board. • A serene watercolor painting of diving board. • A vibrant photo of diving board during sunrise with a warm color palette. • A vivid painting of diving board using vibrant colors. • A cinematic wide-angle shot of diving board at dusk.

Table 16: Prompt samples using different prompt generation methods for the concept *Diving Board* from DomainNet dataset. Irrelevant content, repetitions, and overused phrases are marked in red, brown, and turquoise respectively.

Concept	Method	Examples
The Great Wall of China	LE	<ul style="list-style-type: none"> • The great wall of china was completed • The great wall of china • The Great Wall of the China • The great wall of the province of the city of Beijing • The Wall of China... a building in the countryside
	CHB	<ul style="list-style-type: none"> • The Great Wall of China, wall inside home office • The Great Wall of China, wall inside bakery • The Great Wall of China, wall inside music studio • The Great Wall of China, wall inside subway station • The Great Wall of China wall inside pizzeria
	SC	<ul style="list-style-type: none"> • The Great Wall of China winds majestically through the dense, vibrant greenery of a bamboo forest, creating a striking contrast between ancient architecture and natural beauty. • The Great Wall of China winds majestically through the landscape, surrounded by ancient historical courtyards that echo with the rich history of past dynasties. • The Great Wall of China winds majestically through the dense, vibrant greenery of a bamboo forest, creating a striking contrast between ancient architecture and natural beauty. • Majestic Great Wall of China winding through lush green hills, while sailboats gently glide across a serene lake in the foreground. • The Great Wall of China majestically winds its way through a vibrant, sunny meadow, with lush green grass and colorful wildflowers stretching out in the foreground.
	CCG	<ul style="list-style-type: none"> • The ancient Great Wall of China winds through lush green hills under a bright blue sky. • Tourists wander along the ancient, winding Great Wall of China amidst lush mountains. • Tourists hike along the ancient stone path of the Great Wall winding through green hills. • Visitors hike along the winding, ancient Great Wall of China amidst lush, rolling green hills. • A majestic stretch of ancient stone wall winds over lush, rolling hills under a bright sky.
	HIRPG	<ul style="list-style-type: none"> • A high-contrast black and white photograph of The Great Wall of China. • A serene watercolor painting of The Great Wall of China. • A vibrant photo of The Great Wall of China during sunrise with a warm color palette. • A vivid painting of The Great Wall of China using vibrant colors. • A cinematic wide-angle shot of The Great Wall of China at dusk.

Table 17: Prompt samples using different prompt generation methods for the concept *The Great Wall of China* from DomainNet dataset. Irrelevant content, repetitions, and overused phrases are marked in red, brown, and turquoise respectively.

Method	ID		OOD	
	$A_{AUC} \uparrow$	$A_{last} \uparrow$	$A_{AUC} \uparrow$	$A_{last} \uparrow$
LE	20.01 \pm 0.27	15.38 \pm 0.31	6.40 \pm 0.13	4.59 \pm 0.09
(+) Uncertainty	14.66 \pm 0.30	9.40 \pm 0.14	4.85 \pm 0.08	3.08 \pm 0.06
(+) CRAIG	28.64 \pm 0.55	23.91 \pm 0.27	8.53 \pm 0.27	6.83 \pm 0.07
(+) Glister	17.53 \pm 0.44	11.57 \pm 0.25	5.67 \pm 0.15	3.61 \pm 0.06
(+) GradMatch	27.68 \pm 0.68	22.89 \pm 0.14	8.57 \pm 0.31	6.86 \pm 0.07
(+) AdaCore	24.73 \pm 0.56	18.95 \pm 0.25	7.62 \pm 0.17	5.53 \pm 0.12
(+) LCMat	27.72 \pm 0.49	23.10 \pm 0.23	8.50 \pm 0.22	6.84 \pm 0.02
(+) Moderate	21.33 \pm 0.54	15.91 \pm 0.27	6.47 \pm 0.20	4.56 \pm 0.11
(+) CONAN	30.80\pm0.63	25.33\pm0.20	9.54\pm0.25	7.59\pm0.17
CHB	16.69 \pm 0.16	13.45 \pm 0.19	5.61 \pm 0.11	4.18 \pm 0.05
(+) Uncertainty	11.15 \pm 0.35	7.06 \pm 0.15	3.97 \pm 0.09	2.41 \pm 0.05
(+) CRAIG	26.42 \pm 0.35	22.49 \pm 0.33	8.11 \pm 0.09	6.61 \pm 0.20
(+) Glister	14.07 \pm 0.13	9.38 \pm 0.06	4.68 \pm 0.05	2.98 \pm 0.04
(+) GradMatch	25.20 \pm 0.36	21.58 \pm 0.27	7.97 \pm 0.15	6.51 \pm 0.14
(+) AdaCore	22.29 \pm 0.31	17.27 \pm 0.16	7.23 \pm 0.09	5.27 \pm 0.08
(+) LCMat	24.99 \pm 0.37	21.46 \pm 0.24	7.99 \pm 0.12	6.68 \pm 0.10
(+) Moderate	18.64 \pm 0.24	13.96 \pm 0.10	5.92 \pm 0.07	4.08 \pm 0.06
(+) CONAN	29.06\pm0.37	24.52\pm0.17	9.28\pm0.14	7.56\pm0.14
SC	11.89 \pm 0.17	8.66 \pm 0.20	3.90 \pm 0.07	2.68 \pm 0.04
(+) Uncertainty	10.32 \pm 0.26	6.41 \pm 0.20	3.17 \pm 0.05	1.87 \pm 0.05
(+) CRAIG	20.05 \pm 0.25	17.13 \pm 0.16	6.02 \pm 0.12	4.83 \pm 0.08
(+) Glister	11.30 \pm 0.24	7.24 \pm 0.08	3.42 \pm 0.07	2.10 \pm 0.04
(+) GradMatch	19.83 \pm 0.38	16.82 \pm 0.19	5.94 \pm 0.10	4.78 \pm 0.08
(+) AdaCore	17.67 \pm 0.37	13.29 \pm 0.38	5.19 \pm 0.13	3.69 \pm 0.06
(+) LCMat	19.86 \pm 0.32	16.79 \pm 0.29	5.98 \pm 0.11	4.77 \pm 0.07
(+) Moderate	14.17 \pm 0.24	10.34 \pm 0.06	4.03 \pm 0.07	2.72 \pm 0.05
(+) CONAN	22.36\pm0.34	19.13\pm0.32	6.71\pm0.15	5.48\pm0.13
CCG	12.55 \pm 0.22	10.21 \pm 0.26	4.03 \pm 0.10	2.91 \pm 0.10
(+) Uncertainty	14.73 \pm 0.41	10.65 \pm 0.22	4.48 \pm 0.14	3.13 \pm 0.07
(+) CRAIG	16.72 \pm 0.27	14.23 \pm 0.30	5.16 \pm 0.08	4.11 \pm 0.05
(+) Glister	14.51 \pm 0.38	10.54 \pm 0.15	4.46 \pm 0.12	3.08 \pm 0.03
(+) GradMatch	16.75 \pm 0.26	14.31 \pm 0.21	5.15 \pm 0.11	4.10 \pm 0.07
(+) AdaCore	17.11 \pm 0.36	13.87 \pm 0.18	5.20 \pm 0.14	3.93 \pm 0.11
(+) LCMat	16.71 \pm 0.23	14.08 \pm 0.26	5.15 \pm 0.09	4.05 \pm 0.05
(+) Moderate	14.52 \pm 0.29	11.01 \pm 0.14	4.40 \pm 0.10	3.15 \pm 0.07
(+) CONAN	18.32\pm0.42	15.83\pm0.34	5.78\pm0.17	4.70\pm0.14
HIRPG (Ours)	27.72 \pm 0.30	23.71 \pm 0.39	10.70 \pm 0.19	8.75 \pm 0.13
(+) Uncertainty	21.90 \pm 0.37	15.70 \pm 0.08	10.01 \pm 0.23	7.19 \pm 0.11
(+) CRAIG	32.53 \pm 0.20	28.44 \pm 0.23	13.25 \pm 0.15	11.53 \pm 0.06
(+) Glister	23.16 \pm 0.37	16.98 \pm 0.35	10.56 \pm 0.26	7.60 \pm 0.18
(+) GradMatch	32.53 \pm 0.43	28.36 \pm 0.41	13.48 \pm 0.31	11.74 \pm 0.18
(+) AdaCore	32.15 \pm 0.55	26.83 \pm 0.18	13.62 \pm 0.27	11.37 \pm 0.04
(+) LCMat	32.38 \pm 0.44	28.36 \pm 0.32	13.42 \pm 0.26	11.76 \pm 0.17
(+) Moderate	25.57 \pm 0.42	20.38 \pm 0.16	10.53 \pm 0.29	8.17 \pm 0.13
(+) CONAN (Ours)	34.60\pm0.31	30.09\pm0.11	14.53\pm0.22	12.65\pm0.09

Table 18: **Quantitative comparison between data selection methods with different diverse prompt generation baselines on DomainNet.** Uncertainty, CRAIG, Glister, GradMatch, Adacore, and LCMat require fine-tuning on the full dataset to compute gradient calculations for the fine-tuned model, despite using a pre-trained model for initialization. In contrast, Moderate and CONAN do not require any fine-tuning.